Chapter 3

Nightly Variability of Polarimetric Standard Stars

3.1 Introduction

Nightly, high precision monitoring of polarization standard stars is necessary for calibration of polarized sources. The POLISH instrument on the Hale 5-m telescope is designed to observe polarimetric variability in Cygnus X-1, the most well-studied high mass X-ray binary. This binary is thought to consist of a $40 \pm 10\ M_{\odot}$, O9.7Iab supergiant and a $13.5 - 29\ M_{\odot}$ black hole at a distance of 2.2 ± 0.2 kpc (Ziółkowski 2005). It has a polarimetric period of 2.8 days, which is half the orbital period of 5.6 days (Gies et al. 2003). The amplitude of variability is of order 0.1% in both Stokes Q and U (Kemp et al. 1979, Dolan & Tapia 1989, Wolinski et al. 1996). The spectrum of the strong, linear polarization of order 5% is consistent with interstellar origin (Gehrels 1972, Wolinski et al. 1996), and other members of the Cygnus OB association also share polarization at this level. The intrinsic polarization of the source is due to Thomson scattering by the abundant free electrons from the supergiant as well as Rayleigh scattering from the circumbinary envelope. However, the geometry of the scatterers is poorly understood.

The goal of this observing program is to constrain the orbital inclination of the HDE 226868/Cygnus X-1 supergiant/black hole system and provide a mass estimate for the black hole. In order to constrain the inclination to 5°, however, polarimetric monitoring of Cygnus X-1 must be performed with precision of one part in 10^4 to one part in ten million (Aspin et al. 1981). Systematic effects, especially those that vary on nightly timescales, must be calibrated to this level. Thus, both polarized and unpolarized standard stars must be observed to high precision.

[1]The following paper is derived from observations in this chapter: Wiktorowicz, S. J. 2009, ApJ, in press.

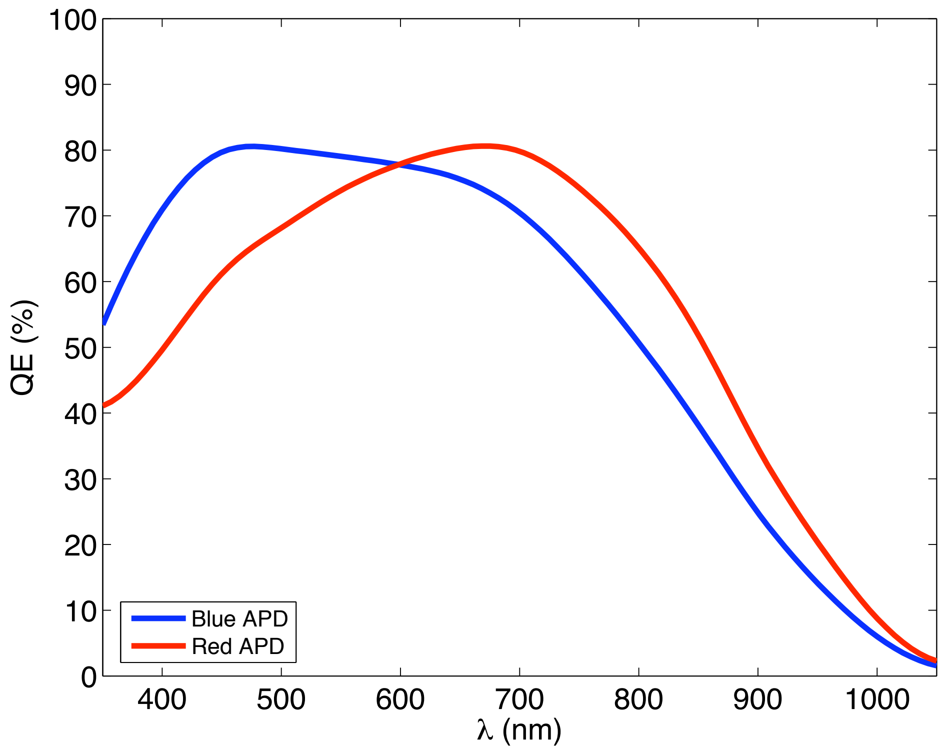

Figure 3.1: Quantum efficiency curves for the red enhanced and blue enhanced APDs (detector 2 and 1, respectively).

3.2 Observations

The POLISH instrument (POLarimeter for Inclination Studies of High mass x-ray binaries/Hot jupiters) is a visible light polarimeter commissioned at the Cassegrain focus of the Hale 5-m telescope at Palomar Observatory, California. This instrument utilizes a photoelastic modulator (PEM) and lock-in amplifiers to modulate and detect incident, polarized light at 100 kHz. These components contribute to the high signal-to-noise observations by the instrument. A Wollaston prism feeds a pair of avalanche photodiodes (APDs) or photomultiplier tubes (PMTs), depending on stellar intensity. Stars with $V < 7$ mag are observed with avalanche photodiodes (see Figure 3.1 for quantum efficiency versus wavelength), while stars fainter than this are observed with photomultiplier tubes. The bandpass of the instrument is limited by the detectors; the lack of spectral filters increases throughput of the instrument and allows for high precision observations. On-source guiding is accomplished by use of a beamsplitter, which allows $\approx 5\%$ of the flux to be sent to a Xybion CCD camera.

Table 3.1: Observed Stars

Name	Alt. Name	RA	Dec	P	Θ (°)	V	Type
Algenib[a]	γ Peg	00 13 14.23	+15 11 00.9	$940.6(5.7) \times 10^{-6}$	111.03(17)	2.83	B2IV
HD 7927	ϕ Cas	01 20 04.92	+58 13 53.8	3.6523(48)%	92.342(87)	5.01	F0Ia
HD 9270	η Psc	01 31 29.07	+15 20 44.8	$105.0(2.9) \times 10^{-6}$	122.3(1.1)	3.63	G7IIa
HR 5854	α Ser	15 44 16.07	+06 25 32.3	$1.84(79) \times 10^{-6}$	–	2.64	K2IIIb
HD 147084	o Sco	16 20 38.18	−24 10 09.6	4.4961(94)%	32.025(97)	4.55	A4II/III
HD 149026[b]	SAO 65349	16 30 29.62	+38 20 50.3	$568.9(7.3) \times 10^{-6}$	80.83(51)	8.16	G0IV
HD 154445	SAO 141513	17 05 32.24	−00 53 31.7	4.5175(32)%	90.318(22)	5.64	B1V
u Her[c]	HD 156633	17 17 19.57	+33 06 00.4	0.1618(15)%	171.90(18)	4.80	B1.5Vp+
γ Oph[d]	HD 161868	17 47 53.56	+02 42 26.3	$178.2(4.0) \times 10^{-6}$	60.56(65)	3.75	A0V
HD 157999	σ Oph	17 26 30.98	+04 08 25.1	1.0482(15)%	85.079(51)	4.34	K3Iab
HD 175541[b]	GJ 736	18 55 40.88	+04 15 55.2	$1117.8(8.3) \times 10^{-6}$	76.96(21)	8.03	G8V
HD 187929[e]	η Aql	19 52 28.37	+01 00 20.4	1.9464(37)%	93.030(67)	$3.5-4.3$	(F6.5−G2)Ib
Cygnus X-1[f]	SAO 69181	19 58 21.68	+35 12 05.8	6.9733(94)%	138.729(33)	8.95	O9.7Iab
HD 189733[b]	V452 Vul	20 00 43.71	+22 42 39.1	$450.7(5.1) \times 10^{-6}$	73.30(34)	7.68	K1.5V
HD 204827	SAO 33461	21 28 57.70	+58 44 24.0	7.9929(97)%	59.542(31)	8.00	O9.5V
HD 212311	SAO 34361	22 21 58.55	+56 31 52.8	$407(27) \times 10^{-6}$	176.37(30)	8.12	A0V
HR 8974	γ Cep	23 39 20.85	+77 37 56.2	$4.6(1.0) \times 10^{-6}$	–	3.23	K1IV

[a] β Cepheid, pulsator
[b] Extrasolar planet host
[c] β Lyrid, eclipsing binary
[d] Debris disk
[e] δ Cepheid, pulsator
[f] High mass X-ray binary

Each on-source measurement consists of one ≈ 30 second integration. Data are sky subtracted by chopping the secondary mirror 25 arcsec due north of the source position. Polarization values are corrected for PEM systematics and then telescope polarization is subtracted. Polarization uncertainty in each measurement is generally two to three times the photon shot noise limit, and night-to-night polarization uncertainty scales according to shot noise statistics. That is, $\sigma_P \propto P^{\frac{1}{2}}$, where σ_P is the polarization uncertainty and P is the stellar polarization. The polarization noise floor of the instrument is about eight parts in ten million for night-to-night observations.

The stars observed are listed in Table 3.1. V band magnitude and spectral type for HD 187929, a δ Cepheid variable, are from Bastien et al. (1988) and Oke (1961) respectively. Spectral type for HD 212311 is from Schmidt et al. (1992). All other non-polarimetric data are from the SIMBAD database. The polarization and position angle values in parentheses represent the standard error of the mean. This is not a measure of source variability; rather, these uncertainties are the square root of the weighted variance of measurements divided by the square root of the number of measurements. Weighting is proportional to number of detected photons to ensure that each detected photon, as opposed to each measurement, is treated equally. This is particularly important when cirrus clouds are present, because observed stellar intensity may vary throughout the night.

The absolute polarization value for each star is related to instrumental gain factors and is not our primary concern. Indeed, we find a correction factor of 0.836 ± 0.064 must be multiplied to polarization measurements from POLISH to make absolute polarization consistent with the Heiles (2000) polarization catalogs. However, this correction factor would increase uncertainty in our measurements unnecessarily. Instead, we aim to discern *relative* changes in polarization with high precision, so this correction factor is not applied to our data.

Cygnus X-1 is known to be variable of order $\Delta P \approx 0.1\%$, and it is included in this paper as a variable control source. This system illustrates the dangers of using the standard error of the mean to determine polarimetric precision of the measurements. That is, Cygnus X-1 is listed in Table 3.1 with a standard error of $\sigma_P \approx 10^{-4}$, which is an order of magnitude lower than the known $\Delta P \approx 0.1\%$ variability. Normalizing the standard deviation of the measurements by the square root of the number of measurements is only valid for normally distributed, i.e., non-variable, data.

3.3 Variability

3.3.1 Intra-Night Variability and Systematic Effects

To determine whether the data from a single night are normally distributed, we use the Kolmogorov-Smirnov (K-S) test. We compare the cumulative distribution function (CDF) of measurements from that night to the CDF for a normal distribution. This test is useful because it makes no assumptions about how the data are distributed, and it is also applicable to data sets of differing size. The benefit of the latter property of the K-S test will become apparent in the next section. The null hypothesis, which posits that the CDF for a given night is randomly distributed, can be rejected if the confidence level α is less than a predetermined value. In this section, rejection of the null hypothesis indicates one, or both, of the following: (1) the star is non-variable on timescales less than one night, and/or (2) systematic effects with timescales less than one night are significant.

In order to generate the CDF for a normal distribution, we first note the definition of the CDF:

$$\mathrm{CDF}\,(Q) \equiv \frac{\int_{-\infty}^{Q} F\,(Q')\,dQ'}{\int_{-\infty}^{\infty} F\,(Q')\,dQ'}. \tag{3.1}$$

The probability density function for normally distributed data is

$$F\left(Q'\right) = \frac{1}{\sigma\sqrt{2\pi}} \exp\left[\frac{-\left(Q' - \overline{Q'}\right)^2}{2\sigma^2}\right]. \tag{3.2}$$

The normalization in Equation 3.2 ensures that the denominator in Equation 3.1 is equal to unity. In Equation 3.2, σ is the standard deviation of the data set, Q', and the mean value of the data set is given by $\overline{Q'}$. Inserting $F\left(Q'\right)$ from Equation 3.2 into Equation 3.1, we find the cumulative distribution function for normally distributed data to be

$$\mathrm{CDF}\left(Q\right) = \frac{1}{2}\left[1 + \mathrm{erf}\left(\frac{Q - \overline{Q}}{\sigma\sqrt{2}}\right)\right]. \tag{3.3}$$

Here, $\mathrm{erf}(x)$ is the error function and is defined as

$$\mathrm{erf}\left(x\right) \equiv \frac{2}{\sqrt{\pi}} \int_0^x e^{-t^2}\, dt. \tag{3.4}$$

To calculate α, we find whether

$$D > \frac{K_\alpha}{\sqrt{n}} \tag{3.5a}$$

$$D > K_\alpha \sqrt{\frac{n_1 + n_2}{n_1 n_2}}. \tag{3.5b}$$

Here, D is the Kolmogorov-Smirnov statistic, which represents the maximum deviation between the CDF from a given night and the CDF expected from the normal distribution. When comparing one data set to a theoretical distribution, Equation 3.5a is used, and Equation 3.5b is used when comparing two data sets. The number of measurements in each data set is given by n, n_1, or n_2. The relationship between K_α and α is

$$\frac{\sqrt{2\pi}}{K_\alpha} \sum_{i=1}^{\infty} \exp\left[\frac{-\left(2i-1\right)^2 \pi^2}{8K_\alpha^2}\right] = 1 - \alpha. \tag{3.6}$$

Measurement of D allows one to solve for K_α in Equation 3.5b, and the confidence level α of non-variability can then be found from Equation 3.6.

Confidence levels of normally distributed, nightly data are listed in Table 3.2. It is convenient to convert α to units of the standard deviation, σ, which is given by $\sqrt{2}\,\mathrm{erf}^{-1}(\alpha)$. Here, $\mathrm{erf}^{-1}(x)$ is the inverse of the error function. Even though only two detectors are used at one time, combining the simultaneous polarization measurement from both detectors is useful. To do this, the weighted mean polarization is taken for each simultaneous pair of measurements. Again, the weighting is proportional to number of photons detected, which is proportional to the signal divided by the detector gain. Combination of measurements from both detectors is referred to as "Detector 1,2".

The range of confidence values across all detectors from Table 3.2, for each star and for each night, are plotted in Figure 3.2. We require normal distribution confidence level to be $< 1\sigma$ to claim variability or significant systematic effects during a single night. However, all nights have roughly the same range of confidence levels, and the upper levels are $> 3\sigma$. Thus, variability and systematic effects on timescales less than one night do not appear to be significant. Figure 3.3 shows each star's confidence levels from Table 3.2 separately. The horizontal, dashed line indicates the 1σ confidence level of normal distribution for a particular star's measurements on a particular night. There appear to be no systematic trends in confidence level seen in all stars during the run, reiterating the conclusion from Figure 3.2 that intra-night systematic effects are not significant.

No stars appear to be significantly variable during a single night. The low confidence levels in both Stokes Q and U for HR 8974 on UT August 5 are inconsistent with the high confidence levels on UT August 3 and 6. Reasons for this are unknown, but it is still likely that polarization from this source is not variable at a detectable level on timescales less than one night. Stokes Q data for HD 147084 do not exist. As stated in section 1, polarization from Cygnus X-1 is known to be variable on the order of $\Delta Q, U \approx 0.1\%$ with a 2.8 day period. Cygnus X-1 observations lasted about three hours per night, so variations of $\Delta Q, U \approx 10^{-5}$ to 10^{-4} are therefore to be expected during each night. However, this variability does not appear to be detected with much confidence, as measurements are distributed randomly to $\approx 2\sigma$ in general.

Table 3.2: Confidence of Random Distribution

UT Date	Star	Q_1 Conf.	Q_2 Conf.	$Q_{1,2}$ Conf.	U_1 Conf.	U_2 Conf.	$U_{1,2}$ Conf.
2007 Aug 3	HR 5854	0.3σ	2.6σ	0.7σ	0.9σ	1.5σ	0.4σ
2007 Aug 4	⋯	2.8σ	1.7σ	2.8σ	2.4σ	2.0σ	3.2σ
2007 Aug 5	⋯	2.6σ	2.2σ	4.0σ	2.0σ	1.8σ	3.6σ
2007 Aug 6	⋯	3.0σ	0.7σ	1.8σ	2.5σ	1.8σ	1.7σ
2007 Aug 3	HR 8974	3.6σ	2.9σ	3.7σ	2.5σ	1.7σ	4.9σ
2007 Aug 4	⋯	–	–	–	3.2σ	4.6σ	2.3σ
2007 Aug 5	⋯	1.7σ	1.5σ	0.6σ	0.5σ	1.7σ	1.8σ
2007 Aug 6	⋯	2.5σ	3.1σ	3.5σ	4.0σ	0.9σ	2.5σ
2007 Aug 4	HD 9270	1.5σ	–	–	1.7σ	–	–
2007 Aug 5	⋯	3.7σ	2.4σ	1.8σ	2.8σ	1.2σ	4.4σ
2007 Aug 6	⋯	1.7σ	1.7σ	2.1σ	2.9σ	1.4σ	3.9σ
2007 Aug 4	γ Oph	0.9σ	1.9σ	2.0σ	1.9σ	2.5σ	4.3σ
2007 Aug 5	⋯	0.5σ	2.4σ	2.2σ	2.3σ	3.4σ	2.5σ
2007 Aug 6	⋯	0.8σ	3.4σ	0.7σ	1.6σ	1.8σ	1.7σ
2007 Aug 3	HD 212311	0.6σ	1.7σ	0.9σ	3.2σ	1.5σ	1.6σ
2007 Aug 4	⋯	1.3σ	1.3σ	3.2σ	2.6σ	2.1σ	2.0σ
2007 Aug 5	⋯	0.8σ	1.0σ	1.7σ	0.2σ	1.2σ	1.6σ
2007 Aug 6	⋯	1.2σ	1.8σ	1.2σ	0.8σ	1.5σ	2.6σ
2007 Aug 5	Algenib	0.9σ	2.0σ	1.9σ	0.2σ	2.7σ	0.6σ
2007 Aug 6	⋯	0.4σ	2.9σ	0.4σ	2.8σ	1.5σ	1.5σ
2007 Aug 5	HD 157999	0.8σ	2.4σ	0.7σ	1.2σ	1.6σ	0.9σ
2007 Aug 6	⋯	1.6σ	0.3σ	1.7σ	1.2σ	2.2σ	1.5σ
2007 Aug 3	HD 187929	2.3σ	1.5σ	2.2σ	1.2σ	0.6σ	0.9σ
2007 Aug 5	⋯	1.4σ	2.7σ	2.1σ	2.5σ	2.5σ	1.5σ
2007 Aug 6	⋯	2.6σ	1.6σ	3.9σ	2.7σ	2.2σ	1.8σ
2007 Aug 3	HD 147084	–	–	–	1.3σ	0.4σ	0.8σ
2007 Aug 4	⋯	–	–	–	1.1σ	3.4σ	1.4σ
2007 Aug 3	HD 204827	2.6σ	2.9σ	3.7σ	1.8σ	2.6σ	2.7σ
2007 Aug 4	⋯	–	–	–	4.2σ	2.4σ	1.4σ
2007 Aug 5	⋯	2.4σ	1.5σ	0.6σ	2.5σ	2.8σ	2.1σ
2007 Aug 6	⋯	1.1σ	1.2σ	1.2σ	2.2σ	3.1σ	1.2σ
2007 Aug 3	Cygnus X-1	2.4σ	1.6σ	1.9σ	1.1σ	2.7σ	2.4σ
2007 Aug 4	⋯	1.0σ	1.2σ	2.4σ	0.3σ	1.8σ	0.8σ
2007 Aug 5	⋯	1.5σ	1.1σ	1.7σ	1.0σ	2.6σ	1.2σ
2007 Aug 6	⋯	0.8σ	0.7σ	0.7σ	0.9σ	1.5σ	2.1σ

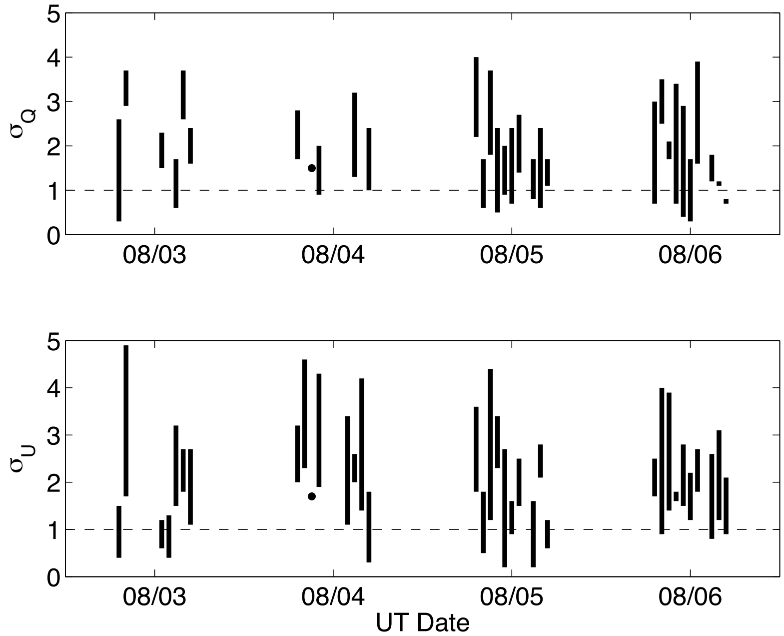

Figure 3.2: Nightly confidence range of normal distribution for all stars. Each vertical line represents the range in confidence level for each star across all detector combinations. Ranges for each star have been displaced from their neighbors in the x-direction for clarity. The points on 2007 Aug 4 are for HD 9270, which only has data from one detector (this can also be seen in Figure 3.3).

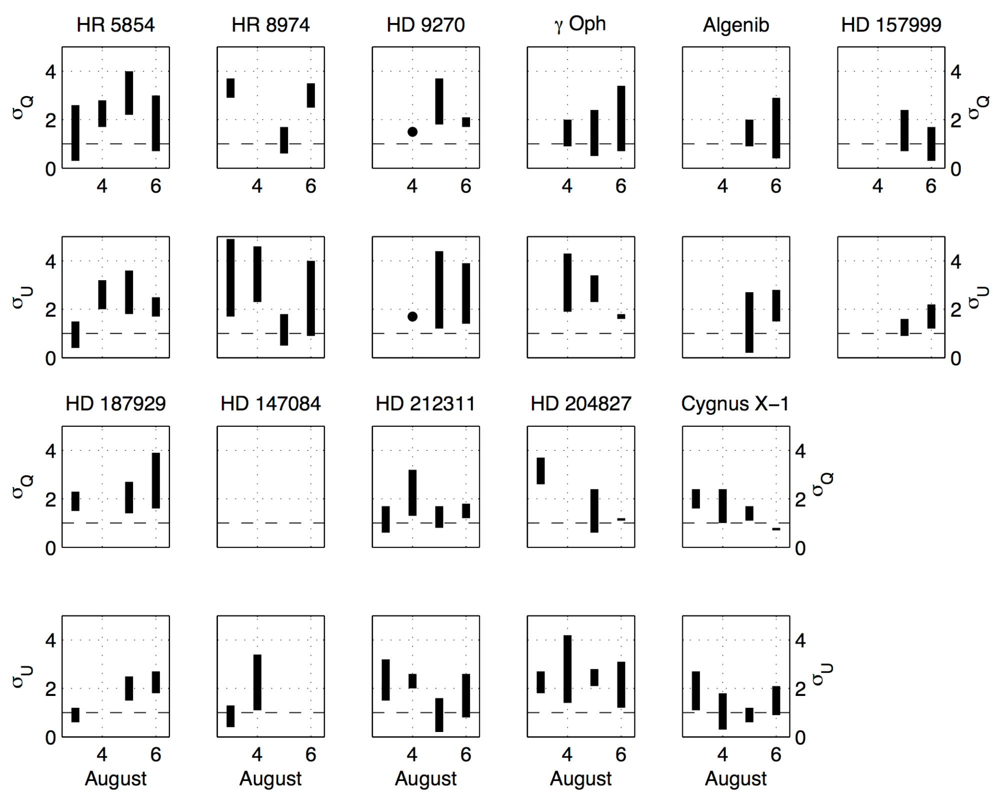

Figure 3.3: Nightly confidence range of normal distribution for individual stars. UT date ranges between 2007 Aug 3 and 2007 Aug 6. Lower values of $\sigma_{Q,U}$ indicate non-random distribution of nightly data.

A hint of intra-night variability in Cygnus X-1 exists for the UT 2007 Aug 6 Stokes Q data, where the confidence of normal distribution ranges from 0.7σ to 0.8σ. Both detector 1 and detector 2 (blue and red enhanced APDs, respectively) agree on this confidence level. However, we do not claim to have detected variability in Cygnus X-1 during this night because (1) the Stokes U confidence ranges for this object do not lie entirely below the 1σ threshold, and (2) the Stokes Q confidence ranges for HD 204827 for that night are also low and tight at 1.1σ to 1.2σ. It appears that some systematic effect caused non-random distribution of data for both of these objects, during this particular night, and only for the Stokes Q data. We currently have no explanation for this.

3.3.2 Night-to-Night Variability

To test for stellar variability over timescales of one night or longer, we compare the CDF of measurements between a pair of nights according to the Kolmogorov-Smirnov (K-S) test. We require $\alpha < 0.01$ in order to reject the null hypothesis and claim stellar variability. Plotted in Figures 3.4 and 3.5 are CDFs measured with each detector, or with the combination of detectors, for the pair of nights listed in the captions. The heavy, solid line is the CDF for the earlier night of the pair, and the thin, solid line is the CDF for the later night. The vertical, dotted line is the D statistic for each pair of CDFs.

To determine extent of polarimetric variability, we find the difference between each weighted mean Stokes parameter for the pair of nights tested. The uncertainty in this variability estimate is the quadrature addition of uncertainties from each night. The uncertainty from each night is taken to be the square root of the weighted variance divided by the square root of the number of measurements. We list α values and polarimetric variability in Tables 3.3 to 3.9. Absolute variability is defined by $\Delta Q, U \equiv Q, U_{\mathrm{night2}} - Q, U_{\mathrm{night1}}$, while relative variability is defined as $\delta Q, U \equiv (Q, U_{\mathrm{night2}} - Q, U_{\mathrm{night1}}) \,/\, |Q, U_{\mathrm{night1}}|$. Weighted mean polarimetric variability $\Delta Q, U_{\mathrm{mean}}$ and $\delta Q, U_{\mathrm{mean}}$ are taken across detector 1, detector 2, and the detector 1,2 combination to determine the likelihood of variability. Here, the weighting is the inverse square of the uncertainty in each detector's estimate of variability. Significant variability is claimed if the following three conditions are met: (1) $\alpha > 0.01$ for both detectors and their combination, (2) ΔQ_{mean} or $\Delta U_{\mathrm{mean}} > 3$ times their uncertainty, and (3) δQ_{mean} or $\delta U_{\mathrm{mean}} > 3$ times their uncertainty.

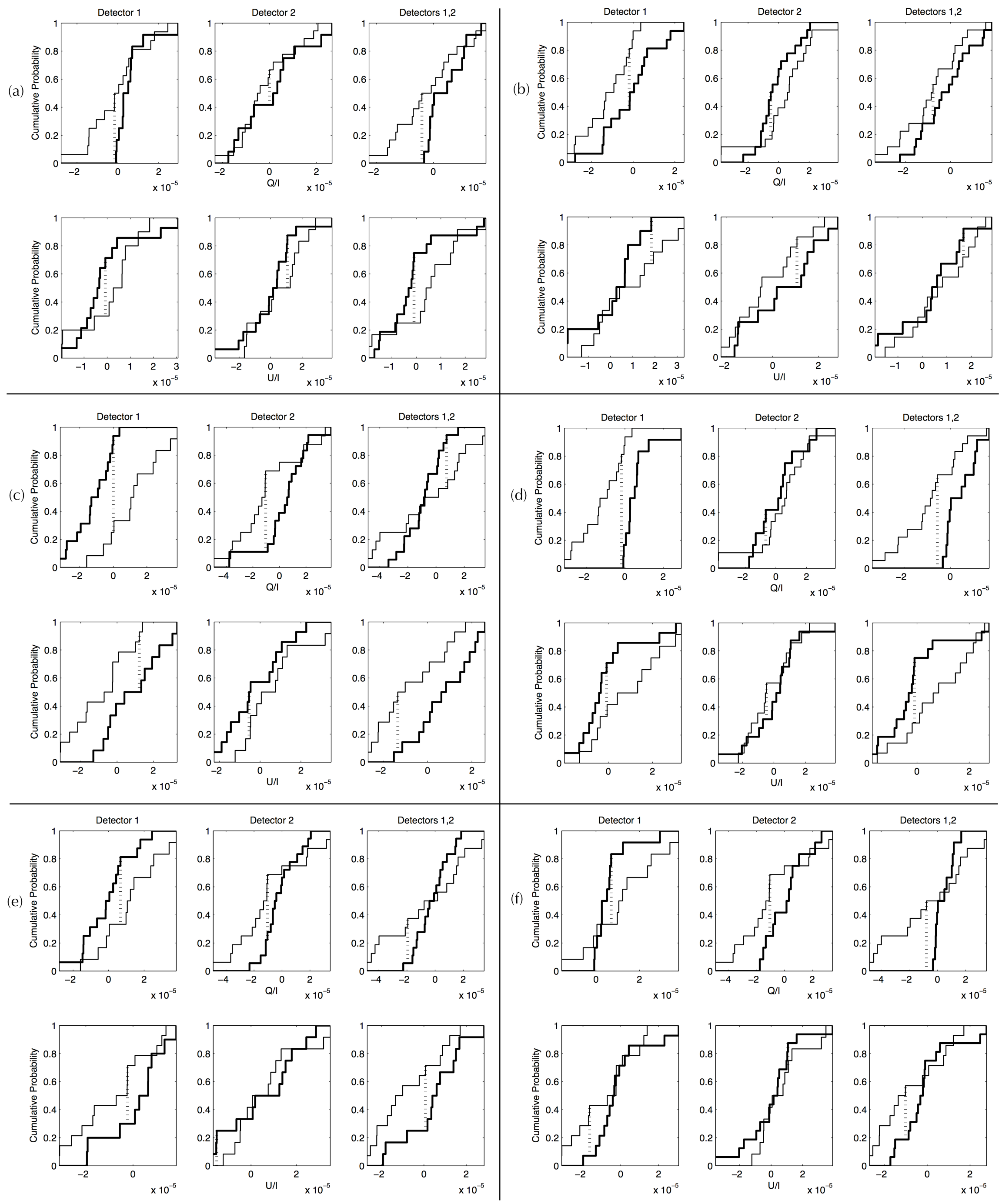

Figure 3.4: CDFs of HR 5854 for 2007 Aug 3 and 4 (a), Aug 4 and 5 (b), Aug 5 and 6 (c), Aug 3 and 5 (d), Aug 4 and 6 (e), Aug 3 and 6 (f).

(a)

(b)

(c)

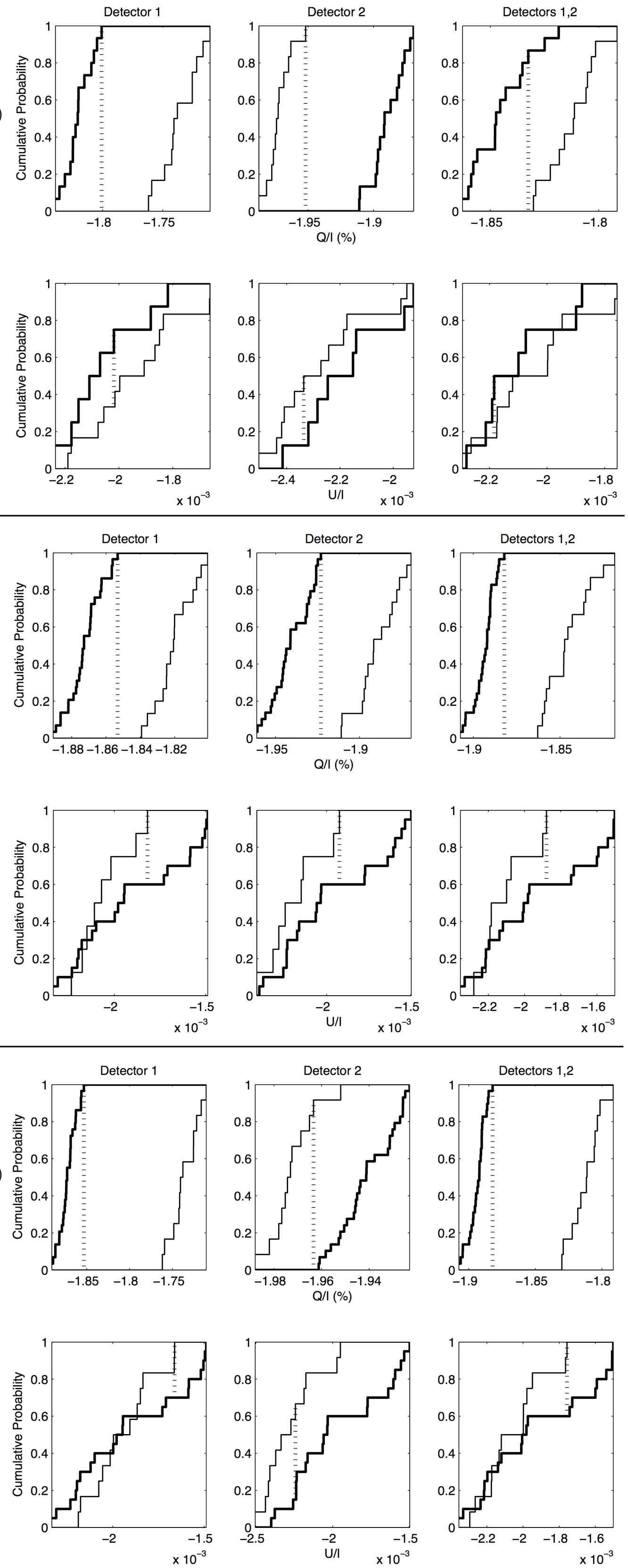

Figure 3.5: CDFs of HD 187929 for 2007 Aug 5 and 6 (a), Aug 3 and 5 (b), and Aug 3 and 6 (c).

Table 3.3: HR 5854 Variability

UT Date ΔNights	2007 Aug 3 1	2007 Aug 4 1	2007 Aug 5 1	2007 Aug 3 2	2007 Aug 4 2	2007 Aug 3 3
α_{Q1}	0.065	0.094	**0.003**	$\mathbf{2 \times 10^{-4}}$	0.086	0.100
α_{Q2}	0.759	0.270	**0.007**	0.759	0.051	0.145
$\alpha_{Q1,2}$	0.055	0.491	0.169	**0.003**	0.353	0.065
α_{U1}	0.269	0.579	0.186	0.305	0.269	0.334
α_{U2}	0.290	0.382	0.469	0.699	0.847	0.927
$\alpha_{U1,2}$	0.065	0.954	0.153	0.080	0.123	0.221
ΔQ_1 $(\times 10^{-6})$	−6.7(5.8)	−12.0(6.9)	**26.3(8.5)**	**−18.7(6.1)**	14.3(8.3)	7.6(7.6)
ΔQ_2 $(\times 10^{-6})$	−2.6(6.3)	1.5(7.2)	−9.3(9.6)	−1.0(7.5)	−7.8(8.7)	−10.4(8.9)
$\Delta Q_{1,2}$ $(\times 10^{-6})$	−5.2(4.8)	−8.3(6.3)	11.1(8.6)	−13.5(5.7)	2.8(8.1)	−2.4(7.6)
ΔQ_{Mean} $(\times 10^{-6})$	**−5.0(1.5)**	−6.6(5.5)	11(14)	−12.4(6.7)	3.4(8.9)	−0.9(7.2)
ΔU_1 $(\times 10^{-6})$	3.1(6.5)	6.1(8.2)	−17.6(9.7)	9.3(7.7)	−11.5(8.8)	−8.4(8.4)
ΔU_2 $(\times 10^{-6})$	5.3(7.6)	−8.5(7.9)	8.2(7.7)	−3.2(7.2)	−0.2(8.1)	5.1(7.4)
$\Delta U_{1,2}$ $(\times 10^{-6})$	3.2(5.8)	2.7(6.6)	−13.1(7.2)	5.9(6.0)	−10.4(7.1)	−7.2(6.5)
ΔU_{Mean} $(\times 10^{-6})$	**3.69(91)**	0.3(5.9)	−6(11)	4.1(4.9)	−7.5(5.0)	−3.5(6)
δQ_1	−1.09(77)	−20(190)	**2.09(70)**	−3.1(1.4)	30(210)	1.2(1.7)
δQ_2	−2.3(6.8)	1.0(4.0)	–	−0.9(5.3)	−5(19)	−9(36)
$\delta Q_{1,2}$	−1.17(88)	−11(61)	1.23(79)	−3.0(1.7)	4(17)	−0.5(1.6)
δQ_{Mean}	**−1.13(11)**	0.98(91)	**1.71(43)**	**−2.96(42)**	−0.1(4.7)	0.31(94)
δU_1	2.5(6.2)	3(12)	−2.2(1.3)	7(21)	−6(14)	−7(25)
δU_2	10(120)	−1.5(1.0)	3.1(4.6)	−6(56)	−0.0(1.4)	10(110)
$\delta U_{1,2}$	4(11)	1.2(4.7)	−2.6(1.9)	7(23)	−4.5(7.3)	−8(36)
δU_{Mean}	**2.73(59)**	−1.31(66)	−2.1(1.2)	6.0(3.4)	−0.24(97)	−6.5(3.1)

Table 3.4: HR 8974 Variability

UT Date ΔNights	2007 Aug 3 1	2007 Aug 4 1	2007 Aug 5 1	2007 Aug 3 2	2007 Aug 4 2	2007 Aug 3 3
α_{Q1}	–	–	**0.003**	**0.003**	–	0.220
α_{Q2}	–	–	**0.005**	0.648	–	**0.001**
$\alpha_{Q1,2}$	–	–	0.020	**0.001**	–	0.404
α_{U1}	0.259	0.236	0.031	$\mathbf{3 \times 10^{-4}}$	0.065	**0.009**
α_{U2}	0.225	0.134	0.189	0.092	0.788	0.094
$\alpha_{U1,2}$	0.948	0.270	**0.002**	0.048	0.032	**0.004**
ΔQ_1 $(\times 10^{-6})$	–	–	**−47(12)**	**32.3(8.6)**	–	−15(10)
ΔQ_2 $(\times 10^{-6})$	–	–	27.6(9.3)	−3.5(7.1)	–	24.1(8.5)
$\Delta Q_{1,2}$ $(\times 10^{-6})$	–	–	−29(11)	**29.4(8.8)**	–	0.7(8.0)
ΔQ_{Mean} $(\times 10^{-6})$	–	–	−10(33)	16(17)	–	5(15)
ΔU_1 $(\times 10^{-6})$	−9.5(6.4)	−14(11)	**68(15)**	−23(10)	**54(13)**	**45(13)**
ΔU_2 $(\times 10^{-6})$	−12.2(7.2)	26(12)	−25(13)	14(12)	1.2(8.8)	−11.0(8.2)
$\Delta U_{1,2}$ $(\times 10^{-6})$	−8.8(5.4)	−9.9(8.1)	**42.7(9.4)**	−18.6(7.4)	**32.9(7.9)**	**24.1(7.2)**
ΔU_{Mean} $(\times 10^{-6})$	**−9.8(1.4)**	−3(15)	29(35)	−13(14)	25(20)	14(21)
δQ_1	–	–	**−1.72(38)**	6.4(5.1)	–	−2.9(4.0)
δQ_2	–	–	5.2(4.6)	−1.9(7.5)	–	13(29)
$\delta Q_{1,2}$	–	–	**−1.12(27)**	7.8(7.3)	–	0.2(2.0)
δQ_{Mean}	–	–	**−1.31(42)**	4.8(3.8)	–	−0.4(1.5)
δU_1	−3.5(4.0)	−2.0(2.7)	3.3(1.2)	−9(11)	8.0(5.6)	17(25)
δU_2	−10(38)	1.91(88)	−2.0(1.0)	11(35)	0.09(63)	−9(34)
$\delta U_{1,2}$	−5.6(9.3)	−1.4(1.7)	**2.50(71)**	−12(21)	4.6(2.4)	15(32)
δU_{Mean}	**−3.90(95)**	1.0(1.5)	1.5(2.1)	−7.8(5.4)	0.5(1.4)	10(11)

Table 3.5: HD 9270 & γ Oph Variability

Star	HD 9270	HD 9270	HD 9270	γ Oph	γ Oph	γ Oph
UT Date	2007 Aug 4	2007 Aug 5	2007 Aug 4	2007 Aug 4	2007 Aug 5	2007 Aug 4
ΔNights	1	1	2	1	1	2
α_{Q1}	0.685	0.584	0.124	0.172	**0.001**	**0.005**
α_{Q2}	–	0.016	–	0.329	0.013	0.172
$\alpha_{Q1,2}$	–	0.873	–	0.035	0.172	0.172
α_{U1}	0.329	0.032	0.251	0.998	0.015	0.004
α_{U2}	–	0.039	–	0.811	0.249	0.094
$\alpha_{U1,2}$	–	0.998	–	0.860	0.109	0.094
ΔQ_1 ($\times 10^{-6}$)	0(12)	−25(15)	−24(13)	4(11)	**46(14)**	**50(14)**
ΔQ_2 ($\times 10^{-6}$)	–	27(16)	–	0.4(9.8)	−29(13)	−28(13)
$\Delta Q_{1,2}$ ($\times 10^{-6}$)	–	−6(13)	–	5.4(8.2)	19(10)	25(11)
ΔQ_{Mean} ($\times 10^{-6}$)	–	−2(20)	–	3.4(2.2)	12(28)	15(31)
ΔU_1 ($\times 10^{-6}$)	−11.4(7.8)	19(11)	8(10)	−2(10)	−40(14)	**−42(13)**
ΔU_2 ($\times 10^{-6}$)	–	−33(17)	–	6(12)	11(12)	17(12)
$\Delta U_{1,2}$ ($\times 10^{-6}$)	–	0.7(9.6)	–	2.2(7.7)	−22(10)	−19.5(9.8)
ΔU_{Mean} ($\times 10^{-6}$)	–	3(17)	–	1.8(2.8)	−16(20)	−15(22)
δQ_1 (%)	1(30)	−62(51)	−61(37)	3.3(9.9)	**45(12)**	**47(12)**
δQ_2 (%)	–	44(23)	–	0(11)	−33(16)	−32(17)
$\delta Q_{1,2}$ (%)	–	−13(32)	–	5.3(7.7)	20(10)	24(10)
δQ_{Mean} (%)	–	14(38)	–	3.6(1.9)	18(27)	23(27)
δU_1 (%)	−12.6(9.1)	19.1(10.0)	9(11)	−1.4(6.4)	**−25.2(8.2)**	**−26.2(7.8)**
δU_2 (%)	–	−41(22)	–	3.5(7.4)	6.9(7.8)	10.7(8.1)
$\delta U_{1,2}$ (%)	–	0.7(9.9)	–	1.4(4.9)	−13.4(6.0)	−12.2(5.9)
δU_{Mean} (%)	–	5(17)	–	1.1(1.7)	−11(12)	−10(14)

Table 3.6: HD 212311 Variability

HD 212311	2007 Aug 3	2007 Aug 4	2007 Aug 5	2007 Aug 3	2007 Aug 4	2007 Aug 3
ΔNights	1	1	1	2	2	3
α_{Q1}	0.423	0.936	0.602	0.560	0.975	0.701
α_{Q2}	0.576	0.883	0.037	0.560	0.478	0.034
$\alpha_{Q1,2}$	0.576	0.739	0.164	0.978	0.070	0.070
α_{U1}	0.112	0.055	0.353	0.665	0.516	0.079
α_{U2}	0.356	0.305	0.959	0.982	0.300	0.966
$\alpha_{U1,2}$	0.969	0.869	0.875	0.665	0.579	0.485
ΔQ_1 (%)	0.001(24)	−0.002(21)	0.011(21)	−0.001(24)	0.009(21)	0.010(24)
ΔQ_2 (%)	−0.019(19)	0.013(18)	−0.042(18)	−0.006(17)	−0.029(21)	−0.048(0)
$\Delta Q_{1,2}$ (%)	−0.010(12)	0.006(10)	−0.018(11)	−0.005(12)	−0.012(11)	−0.022(13)
ΔQ_{Mean} (%)	−0.0105(61)	0.0062(46)	−0.018(17)	−0.0043(17)	−0.011(11)	−0.023(18)
ΔU_1 (%)	−0.046(24)	0.021(24)	−0.024(28)	−0.026(24)	−0.003(28)	−0.049(27)
ΔU_2 (%)	0.040(19)	−0.036(19)	−0.001(23)	0.005(18)	−0.037(24)	0.003(23)
$\Delta U_{1,2}$ (%)	0.003(12)	−0.010(13)	−0.012(15)	−0.008(13)	−0.023(14)	−0.020(14)
ΔU_{Mean} (%)	0.004(27)	−0.012(18)	−0.0112(71)	−0.007(10)	−0.023(10)	−0.019(16)
δQ_1	0.05(79)	−0.06(62)	0.36(81)	−0.02(76)	0.28(74)	0.34(94)
δQ_2	−0.31(27)	0.31(50)	−0.75(27)	−0.09(26)	−0.67(37)	−0.77(25)
$\delta Q_{1,2}$	−0.21(21)	0.15(29)	−0.41(22)	−0.09(23)	−0.32(26)	−0.46(20)
δQ_{Mean}	**−0.236(74)**	0.16(11)	−0.50(24)	**−0.090(16)**	−0.38(25)	−0.56(21)
δQ_1	−2.4(1.5)	0.75(66)	−4(12)	−1.36(97)	−0.1(1.1)	−2.6(1.8)
δQ_2	2.6(1.7)	−1.43(56)	−0.1(2.2)	0.3(1.0)	−1.49(80)	0.2(1.4)
$\delta Q_{1,2}$	5(52)	−5(17)	−1.4(3.1)	−10(200)	−10(38)	−30(470)
δU_{Mean}	−0.1(2.5)	−0.5(1.1)	−0.61(73)	−0.57(83)	−0.99(68)	−0.9(1.4)

Table 3.7: Stellar Variability

Star	Algenib	HD 157999	HD 187929	HD 187929	HD 187929	HD 147084
UT Date	2007 Aug 5	2007 Aug 5	2007 Aug 5	2007 Aug 3	2007 Aug 3	2007 Aug 3
ΔNights	1	1	1	2	3	1
α_{Q1}	$\mathbf{2 \times 10^{-5}}$	$\mathbf{1 \times 10^{-8}}$	$\mathbf{3 \times 10^{-6}}$	$\mathbf{5 \times 10^{-9}}$	$\mathbf{8 \times 10^{-8}}$	–
α_{Q2}	$\mathbf{1 \times 10^{-5}}$	$\mathbf{1 \times 10^{-8}}$	$\mathbf{3 \times 10^{-6}}$	$\mathbf{5 \times 10^{-9}}$	$\mathbf{1 \times 10^{-6}}$	–
$\alpha_{Q1,2}$	$\mathbf{4 \times 10^{-4}}$	$\mathbf{3 \times 10^{-6}}$	$\mathbf{9 \times 10^{-5}}$	$\mathbf{5 \times 10^{-9}}$	$\mathbf{8 \times 10^{-8}}$	–
α_{U1}	0.013	0.037	0.375	0.320	0.509	**0.005**
α_{U2}	0.431	0.211	0.509	0.320	0.036	0.441
$\alpha_{U1,2}$	0.086	0.211	0.660	0.320	0.181	**0.005**
ΔQ_1 ($\times 10^{-6}$)	**−138(22)**	**420(17)**	**849(53)**	**509(34)**	**1358(49)**	–
ΔQ_2 ($\times 10^{-6}$)	**62(10)**	**−544(22)**	**−816(41)**	**506(38)**	**−309(34)**	–
$\Delta Q_{1,2}$ ($\times 10^{-6}$)	**−62(15)**	**143(18)**	**343(46)**	**472(34)**	**815(34)**	–
ΔQ_{Mean} ($\times 10^{-6}$)	3(76)	90(370)	−20(700)	**495(17)**	460(670)	–
ΔU_1 ($\times 10^{-6}$)	34(21)	−99(38)	109(69)	−155(82)	−46(82)	**1000(150)**
ΔU_2 ($\times 10^{-6}$)	−15(11)	94(37)	−144(73)	−182(86)	**−326(83)**	−350(210)
$\Delta U_{1,2}$ ($\times 10^{-6}$)	18(16)	−46(37)	36(68)	−175(82)	−139(82)	**492(63)**
ΔU_{Mean} ($\times 10^{-6}$)	1(20)	−16(81)	10(100)	**−170(11)**	−170(120)	**497(29)**
δQ_1 (%)	**−24.4(4.6)**	**4.09(17)**	**4.66(29)**	**2.72(18)**	**7.25(26)**	–
δQ_2 (%)	**8.5(1.3)**	**−5.10(22)**	**−4.31(22)**	**2.61(19)**	**−1.59(18)**	–
$\delta Q_{1,2}$ (%)	**−10.0(2.6)**	**1.37(17)**	**1.86(25)**	**2.49(18)**	**4.30(18)**	–
δQ_{Mean} (%)	3(10)	0.9(3.5)	−0.0(3.8)	**2.608(95)**	2.4(3.5)	–
δU_1 (%)	5.5(3.3)	−5.5(2.0)	5.3(3.3)	−8.2(4.5)	−2.4(4.4)	**2.51(40)**
δU_2 (%)	−2.4(1.7)	5.0(2.0)	−6.8(3.5)	−9.3(4.7)	**−16.8(4.8)**	−0.84(50)
$\delta U_{1,2}$ (%)	2.9(2.5)	−2.5(2.0)	1.7(3.3)	−9.1(4.6)	−7.3(4.5)	**1.22(16)**
δU_{Mean} (%)	0.3(3.2)	−1.0(4.4)	0.4(4.9)	**−8.88(50)**	−8.4(5.8)	1.22(74)

Table 3.8: HD 204827 Variability

HD 204827 ΔNights	2007 Aug 3 1	2007 Aug 4 1	2007 Aug 5 1	2007 Aug 3 2	2007 Aug 4 2	2007 Aug 3 3
α_{Q1}	–	–	0.013	0.879	–	0.019
α_{Q2}	–	–	0.560	0.602	–	0.483
$\alpha_{Q1,2}$	–	–	0.172	0.725	–	0.212
α_{U1}	0.029	0.071	0.064	0.455	0.864	**0.005**
α_{U2}	0.106	0.183	0.182	0.759	0.677	0.097
$\alpha_{U1,2}$	0.011	0.024	0.025	0.635	0.677	**0.003**
ΔQ_1 (%)	–	–	**−0.059(19)**	0.011(21)	–	−0.048(18)
ΔQ_2 (%)	–	–	−0.021(33)	−0.009(31)	–	−0.030(30)
$\Delta Q_{1,2}$ (%)	–	–	−0.037(20)	0.004(20)	–	−0.033(18)
ΔQ_{Mean} (%)	–	–	**−0.045(14)**	0.0046(71)	–	**−0.0387(77)**
ΔU_1 (%)	**0.175(38)**	**−0.127(37)**	**0.099(31)**	0.048(32)	−0.028(37)	**0.147(32)**
ΔU_2 (%)	**0.091(21)**	**−0.098(24)**	0.061(28)	−0.007(24)	−0.037(25)	0.054(26)
$\Delta U_{1,2}$ (%)	**0.127(22)**	**−0.113(23)**	**0.080(20)**	0.015(20)	−0.033(23)	**0.094(20)**
ΔU_{Mean} (%)	**0.117(29)**	**−0.109(10)**	**0.079(13)**	0.014(19)	**−0.0335(32)**	**0.092(32)**
δQ_1 (%)	–	–	**−1.54(51)**	0.29(54)	–	−1.25(48)
δQ_2 (%)	–	–	−0.54(85)	−0.24(80)	–	−0.78(76)
$\delta Q_{1,2}$ (%)	–	–	−0.97(53)	0.11(52)	–	−0.85(46)
δQ_{Mean} (%)	–	–	**−1.15(37)**	0.12(18)	–	**−1.00(21)**
δU_1 (%)	**2.57(56)**	**−1.81(52)**	**1.44(45)**	0.71(47)	−0.40(53)	**2.16(48)**
δU_2 (%)	**1.28(29)**	**−1.37(33)**	0.86(40)	−0.10(34)	−0.52(36)	0.76(37)
$\delta U_{1,2}$ (%)	**1.83(32)**	**−1.59(32)**	**1.14(29)**	0.21(29)	−0.46(32)	**1.36(28)**
δU_{Mean} (%)	**1.67(43)**	**−1.54(16)**	**1.13(20)**	0.19(28)	**−0.473(41)**	1.32(47)

Table 3.9: Cygnus X-1 Variability

Cygnus X-1 ΔNights	2007 Aug 3 1	2007 Aug 4 1	2007 Aug 5 1	2007 Aug 3 2	2007 Aug 4 2	2007 Aug 3 3
α_{Q1}	$\mathbf{4 \times 10^{-17}}$	$\mathbf{1 \times 10^{-7}}$	$\mathbf{1 \times 10^{-16}}$	$\mathbf{2 \times 10^{-17}}$	$\mathbf{2 \times 10^{-7}}$	$\mathbf{4 \times 10^{-6}}$
α_{Q2}	$\mathbf{3 \times 10^{-16}}$	$\mathbf{2 \times 10^{-5}}$	$\mathbf{6 \times 10^{-13}}$	$\mathbf{6 \times 10^{-17}}$	$\mathbf{2 \times 10^{-5}}$	$\mathbf{6 \times 10^{-5}}$
$\alpha_{Q1,2}$	$\mathbf{2 \times 10^{-16}}$	$\mathbf{7 \times 10^{-8}}$	$\mathbf{6 \times 10^{-17}}$	$\mathbf{7 \times 10^{-17}}$	$\mathbf{4 \times 10^{-7}}$	$\mathbf{8 \times 10^{-8}}$
α_{U1}	$\mathbf{3 \times 10^{-10}}$	$\mathbf{4 \times 10^{-11}}$	$\mathbf{7 \times 10^{-14}}$	0.056	**0.007**	$\mathbf{2 \times 10^{-8}}$
α_{U2}	$\mathbf{1 \times 10^{-17}}$	$\mathbf{1 \times 10^{-16}}$	$\mathbf{1 \times 10^{-18}}$	$\mathbf{3 \times 10^{-4}}$	$\mathbf{8 \times 10^{-6}}$	$\mathbf{4 \times 10^{-14}}$
$\alpha_{U1,2}$	$\mathbf{3 \times 10^{-17}}$	$\mathbf{2 \times 10^{-16}}$	$\mathbf{3 \times 10^{-17}}$	0.016	$\mathbf{4 \times 10^{-6}}$	$\mathbf{1 \times 10^{-16}}$
ΔQ_1 (%)	**−0.210(15)**	**−0.100(15)**	**0.222(14)**	**−0.310(13)**	**0.121(15)**	**−0.089(13)**
ΔQ_2 (%)	**−0.216(18)**	**−0.115(19)**	**0.218(19)**	**−0.331(18)**	**0.103(18)**	**−0.113(18)**
$\Delta Q_{1,2}$ (%)	**−0.216(12)**	**−0.107(13)**	**0.218(13)**	**−0.323(12)**	**0.111(13)**	**−0.105(12)**
ΔQ_{Mean} (%)	**−0.2139(28)**	**−0.1067(55)**	**0.2193(18)**	**−0.3199(80)**	**0.1124(70)**	**−0.1006(97)**
ΔU_1 (%)	**−0.207(24)**	**0.233(24)**	**−0.197(18)**	0.026(21)	0.036(22)	**−0.171(19)**
ΔU_2 (%)	**−0.183(12)**	**0.240(11)**	**−0.175(10)**	**0.057(12)**	**0.065(11)**	**−0.118(12)**
$\Delta U_{1,2}$ (%)	**−0.188(11)**	**0.235(12)**	**−0.1817(98)**	**0.047(10)**	**0.053(11)**	**−0.1352(87)**
ΔU_{Mean} (%)	**−0.1881(68)**	**0.2370(26)**	**−0.1809(69)**	**0.0479(92)**	**0.0563(90)**	**−0.134(15)**
δQ_1 (%)	**−20.2(1.3)**	**−12.1(1.7)**	**30.4(2.3)**	**−29.8(1.1)**	**14.6(2.0)**	**−8.5(1.2)**
δQ_2 (%)	**−19.3(1.4)**	**−12.8(2.0)**	**27.8(2.8)**	**−29.7(1.4)**	**11.4(2.2)**	**−10.1(1.5)**
$\delta Q_{1,2}$ (%)	**−20.2(1.1)**	**−12.6(1.5)**	**29.2(2.1)**	**−30.2(1.0)**	**12.9(1.7)**	**−9.8(1.1)**
δQ_{Mean} (%)	**−19.97(36)**	**−12.46(28)**	**29.26(97)**	**−29.95(23)**	**13.1(1.2)**	**−9.44(69)**
δU_1 (%)	**−3.04(36)**	**3.32(33)**	**−2.90(27)**	0.38(30)	0.51(31)	**−2.51(28)**
δU_2 (%)	**−2.64(18)**	**3.36(15)**	**−2.54(15)**	**0.81(17)**	**0.91(15)**	**−1.71(17)**
$\delta U_{1,2}$ (%)	**−2.74(16)**	**3.32(16)**	**−2.66(15)**	**0.68(14)**	**0.75(15)**	**−1.96(13)**
δU_{Mean} (%)	**−2.73(11)**	**3.343(21)**	**−2.64(11)**	**0.70(13)**	**0.80(12)**	**−1.95(24)**

Most stars are intrinsically unpolarized. For instance, the Sun itself is polarized at the level of less than one part in ten million (Kemp et al. 1987). Polarization of starlight is thought to be caused by interstellar dust clouds along the line of sight. Davis & Greenstein (1951) proposed that elongated dust grains, aligned with their spin axes parallel to the galactic magnetic field, cause preferential extinction of starlight with electric field parallel to the long axis of the grains. Serkowski et al. (1975) discovered an empirical relation to determine whether the polarization of starlight is consistent with origin from interstellar dust. By comparing the wavelength of peak polarization for 364 stars, they find

$$\frac{P\,(\lambda)}{P_{\rm max}} = \exp\left[-1.15\,\ln^2\left(\frac{\lambda_{\rm max}}{\lambda}\right)\right]. \tag{3.7}$$

Here, $P_{\rm max}$ is the maximum polarization as a function of wavelength and $\lambda_{\rm max}$ is the wavelength of maximum polarization. This wavelength is taken to be the mean grain size along the line of sight to the star. Stars with wavelength dependence of polarization lying along this curve are thought to be dominated by interstellar polarization. According to Serkowski et al. (1975), the following stars in our sample are dominated by interstellar polarization: HD 147084, HD 157999, HD 187929, and HD 204827. Additionally, Schmidt et al. (1992) find good fits of their data to interstellar polarization curves for HD 204827. Even Cygnus X-1 appears to owe $\approx 98\%$ of its polarization to interstellar dust grains (Gehrels 1972, Wolinski et al. 1996).

If grain orientation varies along the line of sight, circular polarization will be produced (Serkowski 1962). Additionally, if gain size also varies along the line of sight, position angle of polarization will be wavelength-dependent (Martin 1974). Therefore, the combination of circular polarization and wavelength-dependent linear polarization measurements can constrain grain properties along the line of sight.

Mean polarization versus distance is shown in Figure 3.6. More distant stars tend to have stronger polarization, which is expected if the origin is interstellar. Indeed, all stars in this figure with polarization $P > 1\%$ are dominated by interstellar polarization (cf. Serkowski et al. 1975). Stars with polarization less than this have not been investigated by Serkowski et al. (1975), because they had probably been assumed to be unpolarized. Thus, it is probable that polarization from all stars contains a contribution from the interstellar medium.

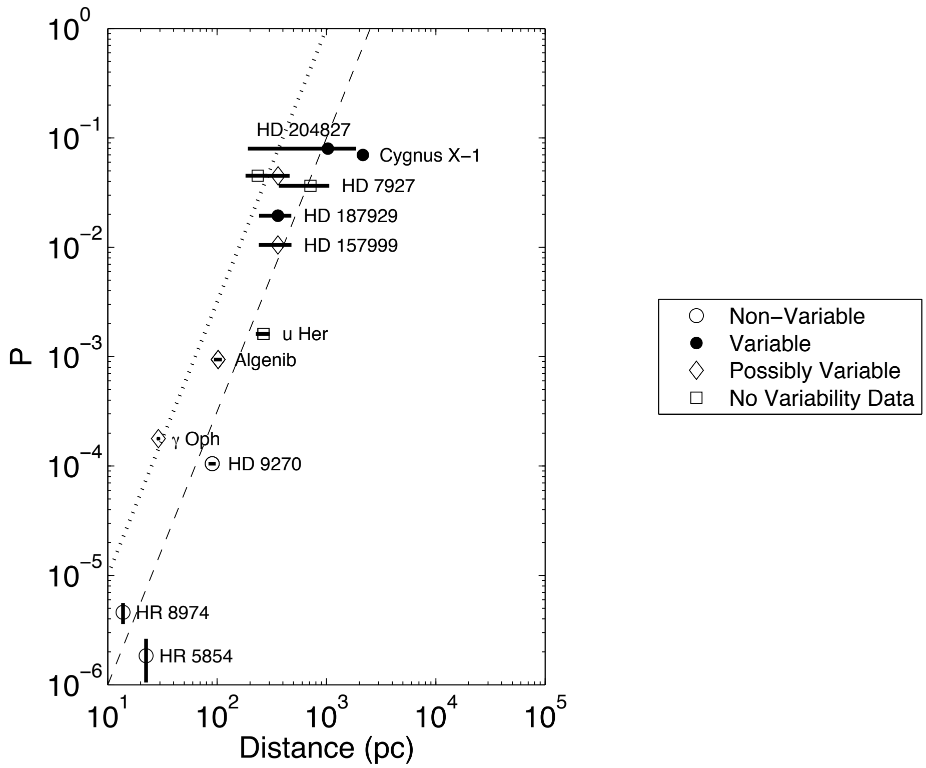

Figure 3.6: Polarization as a function of stellar distance. Stars with only one night of obsevations have also been included. The dashed and dotted lines are guides for the eye.

It is interesting that γ Oph has about an order of magnitude stronger polarization than the dashed trend in Figure 3.6 might indicate. This excess polarization may be due to the debris disk around γ Oph. However, the three stars lying near the dotted trend (γ Oph, HD 154445, and HD 147084) are all close to each other in the sky toward the Galactic Center. This region of enhanced extinction should also have strong interstellar polarization, which should be manifested as a vertical offset to the dashed line.

Similar polarimetric position angle between these three stars would imply that polarization of γ Oph is not due to its debris disk. However, position angles of net polarization are $60.56 \pm 0.65°$, $90.318 \pm 0.022°$, and $32.025 \pm 0.097°$ for γ Oph, HD 154445, and HD 147084, respectively. Thus, there is no common orientation of interstellar dust grains in the lines of sight for these three stars. Indeed, the polarization maps of Mathewson & Ford (1970) show large differences in polarimetric position angle between these stellar locations. The star with no variability data with $P \approx 1\%$ is HD 154445, and the possibly variable star of similar polarization is HD 147084.

However, some stars are intrinsically polarized, evidenced by presence of wavelength-dependent position angle and absence of circular polarization. Intrinsic polarization may be due to circumstellar material or to tidal distortion from binary companions. Polarimetric variability may therefore be caused by intrinsic processes in the stellar atmosphere or surroundings, or it may be caused by changes in the line of sight interstellar medium. A first-order approach to determine the likelihood of ISM variability is to calculate the time taken for a star to traverse its own disk from proper motion, $t_{\rm var}$. Table 3.10 lists proper motions and parallaxes from the SIMBAD database as well as stellar radii R from the Catalog of Apparent Diameters and Absolute Radii of Stars (CADARS: Pasinetti-Fracassini et al. 2001), 3rd Edition. A distance estimate was not found in the literature for HD 212311, so we approximate this by scaling its V band magnitude (from Table 3.1) to the magnitude and distance of γ Oph. This star has a similar spectral type to HD 212311. HD 7927, HD 149026, HD 175541, HD 189733, HD 204827, and HD 212311 are assumed to have radii $R \approx R_\odot$.

Parallax for Cygnus X-1 from SIMBAD is 0.56 ± 1.01 mas, while Ziólkowski (2005) presents a distance of 2.15 ± 0.2 kpc (3σ) for their evolutionary models of this object based on spectroscopy and photometry from Massey et al. (1995). The two values are consistent, but the Massey et al. (1995) value is more precise. We therefore convert the Massey et al. (1995) distance into expected parallax and include in Table 3.10. Stellar radii, R, are from the Catalog of Apparent Diameters and Absolute Radii of Stars (CADARS: Pasinetti-Fracassini et al. 2001), 3rd Edition, for all but HDE 226868 (Cygnus X-1 companion), HD 204827, and HD 212311. The CADARS catalog is obtained through the VizieR Service (Ochsenbein et al. 2000). Radius of HDE 226868 is $22.77 \pm 2.3\ R_\odot$ from Ziólkowski (2005).

Since the bandpasses differ slightly between the red and blue enhanced APDs (Figure 3.1), we attempt to measure change in polarization and position angle for stars observed with APDs. Differences in run-averaged values between detectors are listed in Table 3.11. Difference in P between APDs 2 and 1 is the quadrature addition of the differences in the Stokes parameters. Again, values in bold are significant at the level of three or more times the uncertainty. It can be seen that we detect significant differences in polarization between the APDs for three out of the five stars for which interstellar polarization has been seen. The other two out of five (HD 147084 and HD 154445) show differences in polarization between detector that are significant at 2.4 and 1.6 times the uncertainty, respectively.

We investigate whether differences in polarization from each APD are due to their bandpasses resolving the shape of the interstellar polarization spectrum. Table 3.12 shows that the gain factor necessary to convert our measured Stokes parameters to absolute polarization does not vary between APDs 1 and 2. Therefore, dividing the degree of polarization measured by each APD cancels out any absolute polarization gain factor and takes advantage of our high precision data. We numerically integrate the product of the Serkowski et al. (1975) polarization spectrum from Equation 3.7 with the quantum efficiency of each APD.

The ratio of the integrals from both APDs gives the expected effect of the interstellar polarization spectrum, $(P_2/P_1)_{\mathrm{exp}}$. Values of λ_{max} represent the mean value from the compilation of Serkowski et al. (1975) weighted by the inverse square of the uncertainty. The observed ratios of polarization from both APDs, $(P_2/P_1)_{\mathrm{obs}}$, are also listed. Bold values indicate significant departures from a ratio of unity. We plot the expected and observed ratios of P_2/P_1 in Figure 3.7. The large difference between expected and observed ratios of polarization between the APDs suggests that the differing bandpasses between the APDs may not be significant. The observed ratios seem to be correlated with the expected ratios from the interstellar polarization spectrum, but we currently do not understand the cause of this. Stability of APD1 is known to be far superior to that of APD2, so the anomalously high polarizations detected by APD2 may be a systematic effect.

3.4 Discussion

3.4.1 Standard Stars

HR 5854 (α Ser, HD 140573). No variability estimates were found in the literature for this unpolarized star. While some α, $\Delta Q, U$, and $\delta Q, U$ values in Table 3.3 indicate variability, the large majority indicate this star is non-variable on timescales of one to three nights. This is consistent with the essentially unpolarized nature of this star as well as the minimum ≈ 1 month timescale for significant change in the line of sight ISM column. We find no significant difference in polarization between detectors.

HD 9270 (η Psc, HR 437). The interstellar polarization maps of Mathewson & Ford (1970) show weak polarization in this region of the sky. No variability estimates were found in the literature

Table 3.10: Variability of Interstellar Polarization

Name	P	Θ ($^\circ$)	$\mathrm{PM_{RA}}$ (mas/yr)	$\mathrm{PM_{Dec}}$ (mas/yr)	π (mas)	R (mas)	t_{var} (days)
HR 5854	$1.84(79) \times 10^{-6}$	–	+134.66	+44.14	44.54(71)	4.8	25
HR 8974	$4.6(1.0) \times 10^{-6}$	–	−48.85	+127.19	72.50(52)	3.9	21
HD 9270	$105.0(2.9) \times 10^{-6}$	+122.3(1.1)	+25.73	−3.29	11.09(82)	3.8	107
γ Oph	$178.2(4.0) \times 10^{-6}$	60.56(65)	−23.15	−75.12	34.42(99)	0.61	5.7
HD 212311	$407(27) \times 10^{-6}$	176.37(30)	+21.00	+1.40	≈ 5	≈ 0.02	≈ 0.4
HD 189733	$450.7(5.1) \times 10^{-6}$	73.30(34)	−2.49	−250.81	51.94(87)	≈ 0.2	≈ 0.4
HD 149026	$568.9(7.3) \times 10^{-6}$	80.83(51)	−77.12	+53.34	12.68(79)	≈ 0.06	≈ 0.2
Algenib	$940.6(5.7) \times 10^{-6}$	111.03(17)	+4.7	−8.24	9.79(81)	0.43	33
HD 175541	$1117.8(8.3) \times 10^{-6}$	76.96(21)	−7.84	−89.86	7.8(1.1)	0.027	≈ 0.1
u Her	0.1618(15)%	171.90(18)	−3.68	−5.74	3.77(56)	0.2	21
HD 157999	1.0482(15)%	85.079(51)	+1.25	+7.09	2.78(92)	5.2	530
HD 187929	1.9464(37)%	93.030(67)	+6.94	−7.30	2.78(91)	1.8	130
HD 7927	3.6523(48)%	92.342(87)	−1.31	−2.19	1.40(68)	≈ 0.007	≈ 0.9
HD 147084	4.4961(94)%	32.025(97)	−4.23	−14.71	2.77(76)	1.3	62
HD 154445	4.5175(32)%	90.318(22)	+4.34	−1.91	4.26(96)	0.16	25
Cygnus X-1	6.9733(94)%	138.729(33)	−3.82	−7.62	0.465(43)	0.049	4.2
HD 204827	7.9929(97)%	59.542(31)	−1.21	−2.92	0.97(79)	≈ 0.005	≈ 0.5

Table 3.11: Wavelength-Dependent Polarization

Name	$Q_2 - Q_1$ ($\times 10^{-6}$)	$U_2 - U_1$ ($\times 10^{-6}$)	$P_2 - P_1$ ($\times 10^{-6}$)	$\Theta_2 - \Theta_1$ ($^\circ$)	λ_{max} (nm)	$(P_2/P_1)_{\mathrm{exp}}$	$(P_2/P_1)_{\mathrm{obs}}$
HR 5854	−1.7(4.5)	1.1(4.9)	2.0(4.6)	–	–	–	4(21)
HR 8974	1.8(6.0)	−3.8(6.7)	4.2(6.6)	–	–	–	1.5(2.4)
HD 9270	−7.1(8.4)	1.1(8.9)	7.2(8.4)	1.9(2.3)	–	–	1.023(86)
γ Oph	−6.8(8.2)	**26.9(8.1)**	**27.7(8.1)**	1.2(1.3)	–	–	**1.159(53)**
Algenib[a]	**−52(15)**	−16(10)	**55(15)**	0.75(41)	–	–	**1.055(15)**
u Her	38(28)	−57(32)	69(31)	0.76(55)	–	–	1.033(18)
HD 157999[b]	**−897(58)**	**179(29)**	**915(57)**	0.060(82)	580(30)	1.0094(62)	**1.0899(58)**
HD 187929[b,c]	**−907(77)**	−125(62)	**916(77)**	0.044(93)	546(15)	1.0021(33)	**1.0493(43)**
HD 7927[b,c]	**−960(120)**	−120(170)	**970(120)**	0.03(13)	511.9(3.9)	0.99445(91)	**1.0266(34)**
HD 147084[a,b]	660(310)	**260(75)**	710(290)	0.30(17)	664.0(8.0)	1.0256(14)	**1.0115(34)**
HD 154445[b]	−240(340)	300(130)	390(240)	0.192(86)	573(49)	1.008(10)	1.0053(76)

[a]Circular polarization detected
[b]Interstellar P versus λ
[c]Rotation of θ versus λ

Table 3.12: Corrections for Absolute Polarization

Parameter	APD1	APD2	Mean	PMT1	PMT2	Mean
$P_{\mathrm{POLISH}} - P_{\mathrm{Heiles}}$ ($\times 10^{-4}$)	1.8(3.6)	1.8(3.8)	1.8438(21)	8(35)	9(37)	8.84(53)
$P_{\mathrm{POLISH}}/P_{\mathrm{Heiles}}$	0.843(87)	0.842(62)	0.84224(69)	0.690(20)	0.672(22)	0.6811(89)

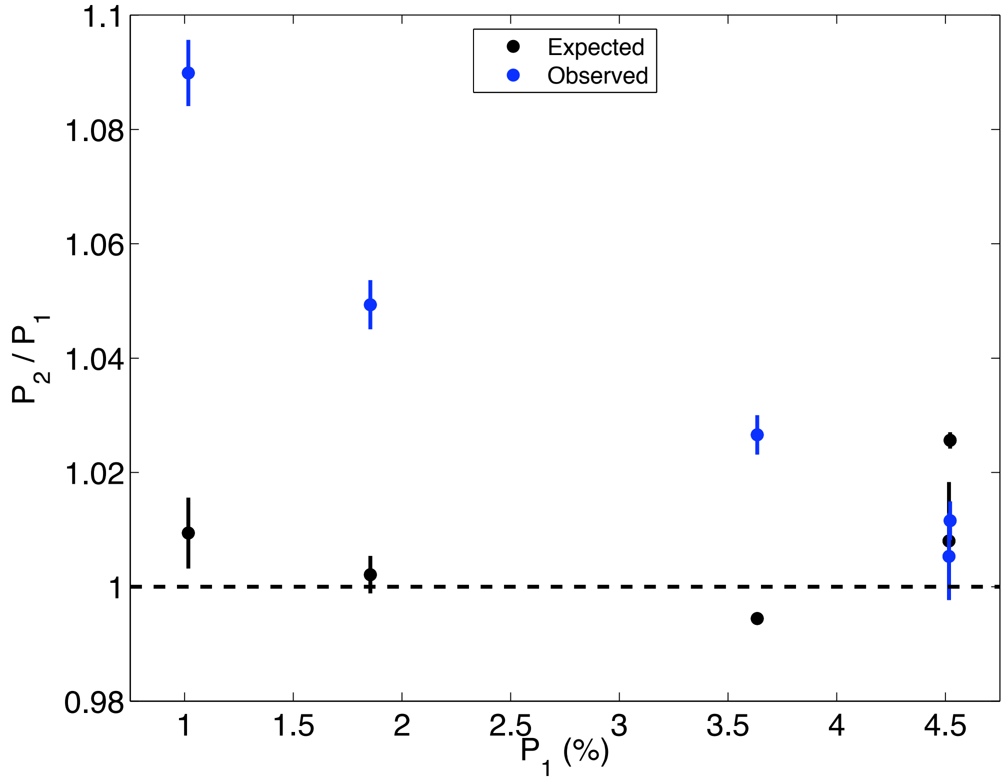

Figure 3.7: Expected and observed ratios of polarization between APDs.

for this weakly polarized star. HD 9270 is not significantly variable on one to two night timescales according to Table 3.5, and lack of detected variability is expected due to its weak polarization. The minimum ≈ 3.5 month timescale for significant ISM change in the line of sight to HD 9270 is expected to inhibit variability for the duration of our observations. We find no significant difference in polarization or position angle between detectors.

HD 212311. This weakly polarized star is classified as an unpolarized standard according to Schmidt et al. (1992), who report B and V band polarizations of $(2.8 \pm 2.5) \times 10^{-4}$ and $(3.4 \pm 2.1) \times 10^{-4}$, respectively. We also detect linear polarization of order one part in 10^4, but it is detected at the 15σ confidence level. We therefore caution against the use of HD 212311 as an unpolarized standard. Because of its weak polarization, we do not expect significant changes in polarization to be detected. Indeed, Schmidt et al. (1992) claim it is non-variable, and we confirm non-variability up to our detection limit on one to three night timescales, as seen in Table 3.6.

u Her (HD 156633). Rudy & Kemp (1977) find phase-locked polarization modulation of amplitude 0.03% in this partially eclipsing binary with two day period (Kukarkin et al. 1958). Orbital inclination is 76° (Batten 1967) to 77° (Merril 1963), and the secondary appears to fill its Roche lobe (Merril 1963, Kovachev & Reinhardt 1975). By assuming intrinsic polarization to be zero at conjunctions, Rudy & Kemp (1977) assert the interstellar polarization to be 0.02% to 0.03%. The minimum timescale for significant ISM variability is $\approx$ 1 month, which proves that variability in u Her is intrinsic. Unfortunately, our observations only span one night, so we are unable to comment on variability.

HD 157999 (σ Oph, HR 6498). Serkowski et al. (1975) find wavelength dependence of polarization consistent with interstellar origin. No variability estimates were found in the literature for this polarized star. HD 157999 appears to be significantly variable in Stokes Q on a one night timescale (Table 3.7), but the signs of variability ΔQ and δQ vary between detector. This star may be variable from night to night, but we do not have enough data to state this with much confidence. The minimum timescale for ISM column variability of $\approx$ 1.5 years requires that polarimetric variability, if subsequently confirmed, must be intrinsic to the star.

Variability estimates for HD 157999 are preferentially stronger in Stokes Q than in Stokes U. Since the highest signal to noise ratio is achieved on the Stokes parameter with highest polarization, variability in this Stokes parameter will be most easily detected. HD 157999 has polarimetric position angle $\Theta \approx 90°$, so Stokes Q is an order of magnitude stronger than Stokes U. This is most likely the reason for strong Stokes Q variability and weaker Stokes U variability.

HD 7927 (ϕ Cas, HR 382). Serkowski et al. (1975) find significant interstellar polarization in the line of sight to this star based on the wavelength dependence of polarization. Many authors (Gehrels & Silvester 1965, Coyne & Gehrels 1966, Hsu & Breger 1982, Dolan & Tapia 1986, Bastien et al. 1988, Wolff et al. 1996) find significant wavelength dependence of position angle. Dolan & Tapia (1986) and Bastien et al. (1988) claim nightly variability of this star and interpret it to be intrinsic in origin. However, Clarke & Naghizadeh-Khouei (1994) reject the variability claim of Bastien et al. (1988) on the grounds that their statistical analyses lacked rigor. They perform a K-S test on the cumulative distribution function of position angle to claim non-variability of this star. Bastien et al. (2007) re-analyze the Bastien et al. (1988) data and assert that variability exists. Unfortunately, our observations only span one night; therefore, we cannot comment on variability of HD 7927.

HD 147084 (o Sco, HR 6081). Both Martin (1974) and Serkowski et al. (1975) find wavelength-dependent linear polarization consistent with interstellar origin. Dolan & Tapia (1986) observe low significance changes in polarimetric position angle Θ with wavelength: their probability of constant Θ versus wavelength is 0.35 according to the χ^2 test. While their uncertainty in position angle for this star is substantially larger than other stars in their program, the lack of wavelength dependence on position angle is supported by many authors (Serkowski 1968, Serkowski et al. 1975, Hsu & Breger 1982, Bailey & Hough 1982, Clarke 1986).

However, Kemp (1972) and Kemp & Wolstencroft (1972) detect significant wavelength-dependent circular polarization in the line of sight to this star. Martin (1974) further finds the wavelength dependence of circular polarization to be consistent with significant change in grain orientation along the line of sight. Reconciliation of the lack of wavelength dependence on position angle as well as the presence of significant circular polarization can occur by two effects. Either grain orientation but not size varies along the line of sight, the star possesses intrinsic polarization, or both.

Dolan & Tapia (1986) posit that the star is intrinsically polarized, and they hypothesize that this intrinsic polarization has wavelength dependence on position angle opposite that due to the line of sight dust grains. This hypothesis may be supported by the timescale of variability seen by Bastien et al. (1988) as well as by the reanalysis by Bastien et al. (2007). In Figure 2 of Bastien et al. (1988), variability in degree of polarization as well as position angle seems to occur over the first nine-night interval. Consultation of Table 3.10 shows that ISM variability requires at least two months to be detected, implying that the source of variability may be intrinsic. On the other hand, the remaining ≈ 31 nights in Figure 2 of Bastien et al. (1988) do not show much variability. Additionally, Clarke & Naghizadeh-Khouei (1994) criticize the Bastien et al. (1988) assertion of variability. A simpler explanation of the lack of wavelength-dependent position angle is that grain size may not change in the line of sight. Unfortunately, we have no Stokes Q measurements, and the variability in Stokes U changes sign between our detectors (Table 3.7). Therefore, our data are not sufficient to confirm variability of Bastien et al. (1988) or to otherwise shed light on this subject.

HD 204827. Serkowski et al. (1975) find polarization of this star to be caused by the ISM. Hsu & Breger (1982) see significant change in position angle with wavelength. Dolan & Tapia (1986) also observe changes in polarimetric position angle Θ with wavelength: their probability of constant Θ versus wavelength according to the χ^2 test varies from $\alpha = 0.09$ to $\alpha < 10^{-5}$ over a two month interval. However, Schulz & Lenzen (1983) claim that no significant rotation of position angle occurs with wavelength. A χ^2 analysis of their $UBVRI$ band data gives the probability of constant position angle to be $\alpha = 0.07$. Clayton et al. (1995) also claim that no substantial change in position angle occurs with wavelength, but their Figure 1 clearly shows the trend of increasing position angle with increasing wavelength seen by Hsu & Breger (1982) and Dolan & Tapia (1986). Indeed, they perform no statistical tests to verify their claim. No circular polarization measurements were found in the literature.

Three authors classify this strongly polarized star as variable on a ≈ 4 night timescale (Dolan & Tapia 1986, Bastien et al. 1988, reanalysis by Bastien et al. 2007), but Schmidt et al. (1992) claim it is not. Additionally, Clarke & Naghizadeh-Khouei (1994) criticize the variability claim of Bastien et al. (1988). We observe significant changes in Stokes U (ΔU_{mean} and δU_{mean} in Table 3.8) on timescales of one to three nights. However, the cumulative distribution functions do not significantly vary on one and two night timescales ($\alpha_U > 0.01$), but they do significantly vary on a three night timescale. The few nights for which Stokes Q data exist show significant variability in ΔQ_{mean} and δQ_{mean} as well, but again the CDFs do not significantly vary. Therefore, we confirm variability of this star on a three night timescale and suspect it to be present on shorter timescales, but further data are required for confirmation. The minimum timescale for ISM variability is of order one day from Table 3.10, which raises the possibility of polarimetric variability due to the ISM.

3.4.2 Extrasolar Planets

HR 8974 (γ Cep, HD 222404). No variability estimates were found in the literature for this unpolarized star. The primary component of the binary system with period 67.5 ± 1.4 years (Neuhäuser et al. 2007) harbors an extrasolar planet. Hatzes et al. (2003) discovered a planetary companion to the primary star, and the minimum 1.60 ± 0.13 Jupiter mass planet has a period of $T \approx 903$ days and semimajor axis $a \approx 2.04$ AU (Neuhäuser et al. 2007). Therefore, we expect the amplitude of the planetary polarimetric signal to be of order 10^{-8} or less and consequently undetectable. This star does not appear to be significantly variable on one to three night timescales, as seen in Table 3.4. This is consistent with the essentially unpolarized nature of this star as well as the minimum ≈ 1 month timescale for significant change in the line of sight ISM column. We find no significant difference in polarization between detectors.

Table 3.13: Variability of Exoplanet Host Stars

Name	System Properties M (M_J)	T (days)	a (AU)	i (°)	Stokes	χ^2/n	α	$\frac{1}{2}\Delta(Q,U)$ (10^{-5})
HD 189733[a]	1.150(46)	2.2185733(20)	0.0312(4)	85.76(29)	Q/I	6.7/6	0.353	4.7(3.2)
...	...	...	...	...	U/I	6.9/6	0.329	4.8(2.7)
HD 149026[a]	0.36(3)	2.8758887(35)	0.0432(6)	$85.4^{+0.9}_{-0.8}$	Q/I	2.3/7	0.942	3.2(2.3)
...	...	...	...	...	U/I	5.8/7	0.560	7.6(4.1)
HD 175541	$0.61 \sin i$	297.3(6.0)	1.03	?	Q/I	5.4/6	0.492	5.4(2.7)
...	...	...	...	...	U/I	9.1/6	0.168	6.2(2.4)
HR 8974	$(1.60 \pm 0.13) \sin i$	902.9(3.5)	2.044(57)	?	Q/I	2.9/3	0.401	1.47(86)
...	...	...	...	...	U/I	0.6/4	0.965	0.26(41)

[a]Transiting planet

HD 175541. No variability estimates were found in the literature for this weakly polarized star. It harbors a planet with minimum mass 0.61 Jupiter masses, a period of $T \approx 297$ days, and semimajor axis 1.03 AU (Johnson et al. 2007). Since the fraction of starlight intercepted by the planet is less than one part in 10^7, any observed polarimetric variability from the system cannot be due to the planet. Constant polarization of this system over six nights can only be rejected at the $\alpha = 17\%$ level of significance according to the χ^2 test (Table 3.13 and Figure 3.8). We require $\alpha < 1\%$ in order to confirm variability of the star. Therefore, we cannot claim variability of HD 175541 with confidence; however, Figure 3.8 shows qualitative evidence of a long-period trend in the polarization of this star. This may be due to variability in the ISM, because the minimum timescale for this process is less than one day.

HD 149026. No variability estimates were found in the literature for this weakly polarized star. A short-period, transiting planet exists around this star with $M = 0.36 \pm 0.03\ M_J$ (Winn et al. 2008), $T \approx 2.9$ day period, semimajor axis $a \approx 0.04$ AU, and $i = 85.4^{+0.9^\circ}_{-0.8^\circ}$ (Nutzman et al. 2008). Constant polarization of this system can only be rejected at the $\alpha = 56\%$ level of significance; therefore, we do not observe significant variability (Table 3.13 and Figure 3.9). It is interesting to note that the Stokes U observations near phase 0.8, where phase 0 is set to be mid-transit, are somewhat different from each other. Therefore, there does not appear to be strong phase-locking of the polarization of the system to the orbital period of the planet. This is expected from a system where the planet only intercepts of order one part in 10^5 of the stellar flux; consequently, the polarimetric amplitude of the system from the transiting planet is expected to be one part per million to one part in ten million.

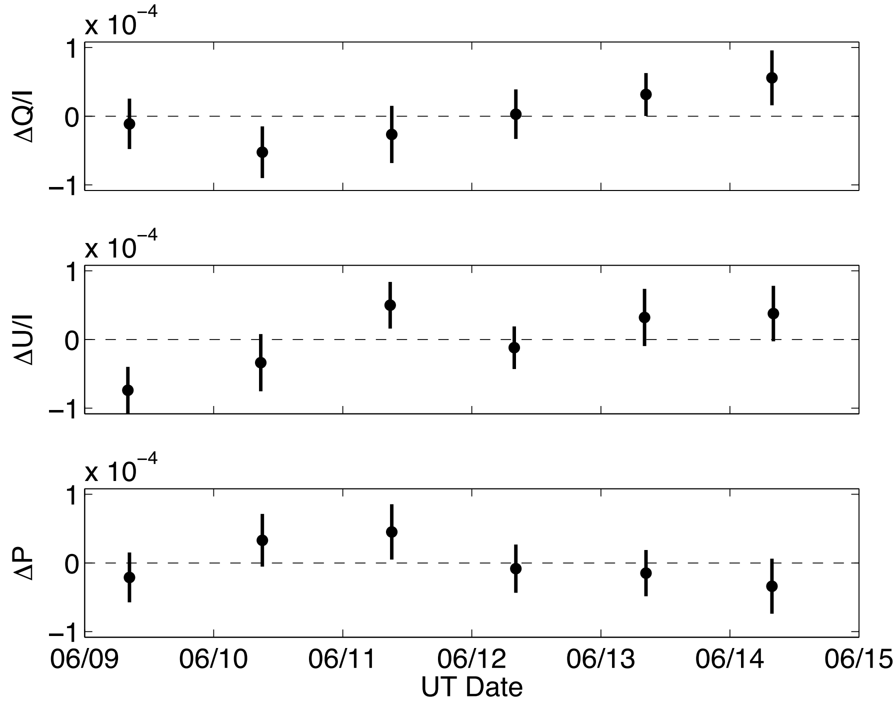

Figure 3.8: Observed polarization of the HD 175541 exoplanet system. Mean polarization of order one part in 10^4 has been subtracted.

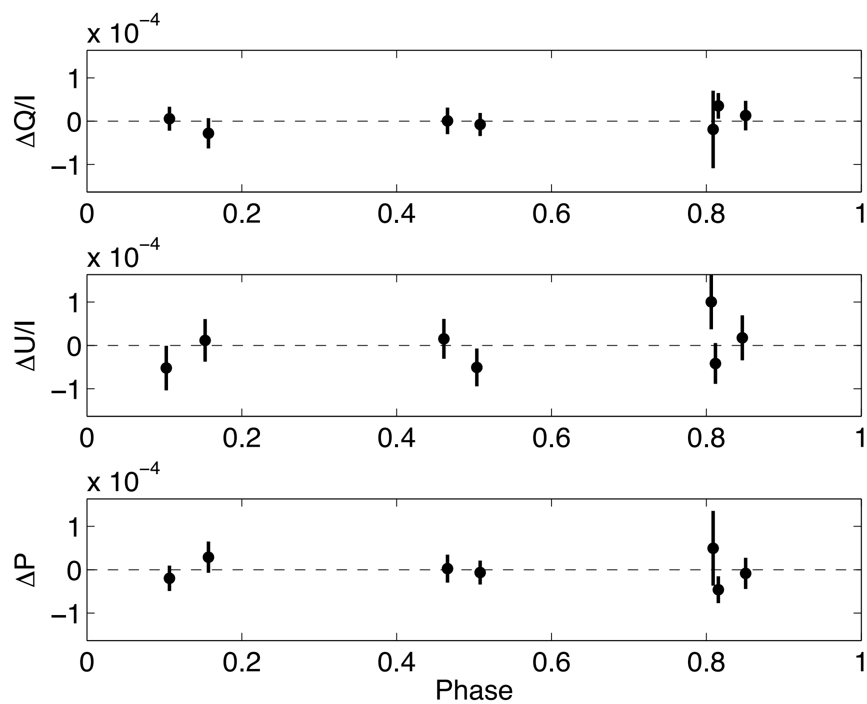

Figure 3.9: Observed polarization of the HD 149026 transiting hot Jupiter system. Mean polarization of order one part in 10^4 has been subtracted. Phase 0 represents mid-transit (0.5 phase difference between transit and radial velocity ephemerides).

HD 189733 (V452 Vul). Berdyugina et al. (2008, hereafter B08) observe marginal variability of this system, which harbors a transiting hot Jupiter with $M = 1.150 \pm 0.046\ M_J$, $T \approx 2.2$ days, $a \approx 0.03$ AU, and $i = 85.76 \pm 0.29°$ (Winn et al. 2007). They attribute this modulation to stellar flux scattered by the hot Jupiter. However, planetary polarization is expected to be only of order one part per million or less, especially when multiple scattering in the planetary atmosphere is taken into account (cf. Seager et al. 2000). The polarimetric modulation of HD 189733 appears to be two orders of magnitude larger than expected from a planetary origin, where B08 observe $\Delta P \approx 2 \times 10^{-4}$. Indeed, in order to explain this large of a modulation from scattering by a planetary atmosphere, B08 invoke a Lambertian sphere, with geometric albedo of 2/3. Even with this unrealistically large albedo, B08 require a planetary radius 30% larger than the radius measured by transits. The ratio of planetary to stellar radii is accurately obtained from transit observations, and near-IR interferometry has accurately determined the stellar radius (Baines et al. 2007). Planetary radius estimates from transit and interferometric observations are more reliable than the polarimetric estimate by B08. Therefore, the polarimetric modulation observed by B08 cannot be due to the planet.

A potential cause of polarimetric variability in hot Jupiter host stars is starspot activity. Photometric observations by the MOST satellite suggest the existence of starspots on the short period τ Boö that follow the rotation period of the star (Walker et al. 2008). There is also some evidence that Ca II H and K emission from the short period HD 179949 may follow the stellar rotation period (Shkolnik et al. 2005, 2008). HD 187933 is known to be active, with up to 1% of its surface covered in spots at any time (Hébrard & Lecavelier des Etangs 2006, Croll et al. 2007, Pont et al. 2007, Winn et al. 2007, Moutou et al. 2008). These spots appear to rotate with the roughly 11.8 day stellar rotation period (Henry & Winn 2008, Croll et al. 2008). Unfortunately, B08 do not discuss the probability of starspots causing their observed modulation.

Plotted in Figure 3.10 are the phase-binned observations of B08. They observe polarization peaks at quadrature phases and vanishing polarization at conjunctions. B08 take these observations to be evidence of a planetary origin of the polarimetric signature of the system. That is, a planet at quadrature ensures a 90° scattering angle, which maximizes the degree of polarization from the planet. At conjunctions, however, a planet is at near-full or near-new phase, which generates zero net polarization. However, the Lambertian planetary model of B08 fails to accurately describe the Stokes U variability near phase 0.2 (Figure 3.10). This may be evidence of the more complex polarization modulation due to a corotating, polarized starspot. While the ISM may be variable on a timescale less than the orbital period of the planet, the consistent but weak variability observed by B08 and POLISH at these phases suggests that ISM variability is not the cause of observed modulation in HD 189733.

In Figure 3.11, we show nightly mean polarization of HD 189733 observed with POLISH. There appears to be qualitative variability in our polarimetric observations, which is similar to that observed by B08. However, since constant polarization can only be rejected at a χ^2 significance of $\alpha = 33\%$, variability cannot be confirmed. Like B08, we observe increases in both Stokes Q and U during this phase. When plotting $\Delta P = \sqrt{(\Delta Q/I)^2 + (\Delta U/I)^2}$, which is the degree of "excess" polarization after mean polarization in each Stokes parameter is removed, we find weak evidence for an increase in degree of polarization near quadrature. We also find weak evidence for a low degree of polarization near phase 0.5, which is defined to be inferior conjunction of the star. At this phase, a corotating starspot will lie behind the stellar limb, so a decrease in polarization near phase 0.5 does not prove a planetary origin for the polarimetric modulation. Longer phase coverage of the polarimetric modulation of the system is required to determine the existence of a polarized starspot.

Because of the high degree of polarization of flux scattered through 90°, a stellar limb is expected to be polarized. The position angle of limb polarization is expected to be tangent to the limb, because the scattering plane is in the radial direction. Outside of a transit, the symmetry of main sequence stellar disks ensures low net intrinsic stellar polarization. However, as a planet contacts the limb of a star to mark the beginning of a transit, the partial occultation of the star's limb generates net polarization. The partial loss of polarization tangent to the stellar limb causes net polarization of the starlight parallel to the line connecting the centers of the planet and star (Figure 3.12). During mid-transit, the polarization vector is perpendicular to the orbital plane, but the degree of polarization is low. This is because stellar polarization is concentrated in the limb. For $83° < i < 90°$, the planet will transit at mid-latitudes on the star, so the North/South Polar limb will not be occulted. Thus, the maximum change in polarization during the transit will take place at ingress and egress, as opposed to mid-transit.

The strength of the polarimetric modulation during the transit has been modeled by Carciofi & Magalhães (2005), which is presented as our Figure 3.13. The amplitude varies over two orders of magnitude, from one part per million to one part in 10^4, depending on the strength of the stellar limb polarization, its radial dependence, and the wavelength observed. The strongest signal appears

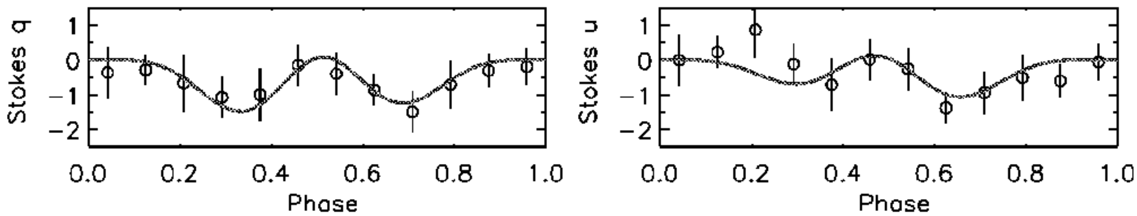

Figure 3.10: Polarimetric modulation of the HD 189733 transiting hot Jupiter system from Figure 1 of Berdyugina et al. (2008). Mean polarization of order one part in 10^4 has been subtracted.

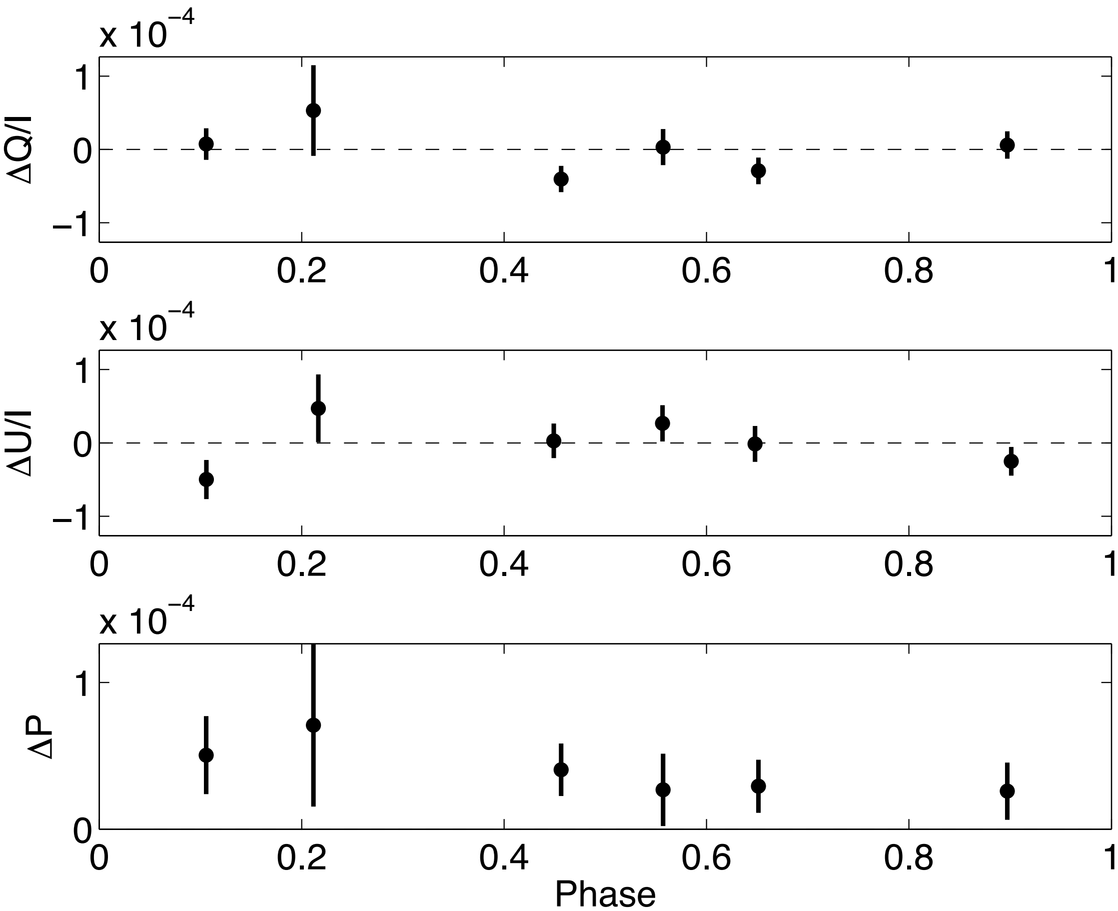

Figure 3.11: Observed polarization of the HD 189733 transiting hot Jupiter system. Mean polarization of order one part in 10^4 has been subtracted. Phase 0 represents mid-transit (0.5 phase difference between transit and radial velocity ephemerides).

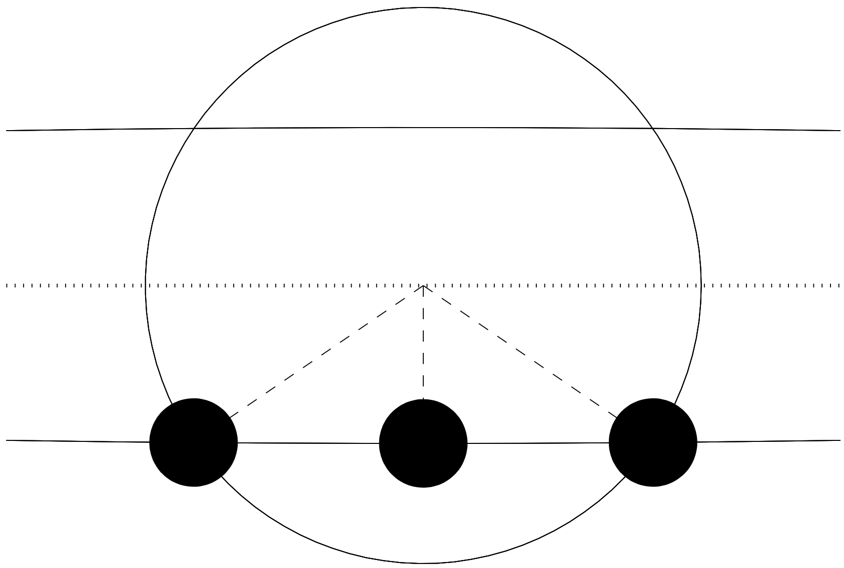

Figure 3.12: HD 189733 transit geometry, planet and star are to scale. Dashed lines indicate position angle of net polarization at transit ingress, mid-transit, and egress. A degeneracy exists in photometry between a Northern and Southern Hemisphere transit, where the dotted line indicates the equatorial plane of the star. Polarimetry appears to have resolved this degeneracy: a Southern Hemisphere transit (pictured) is consistent with the observations.

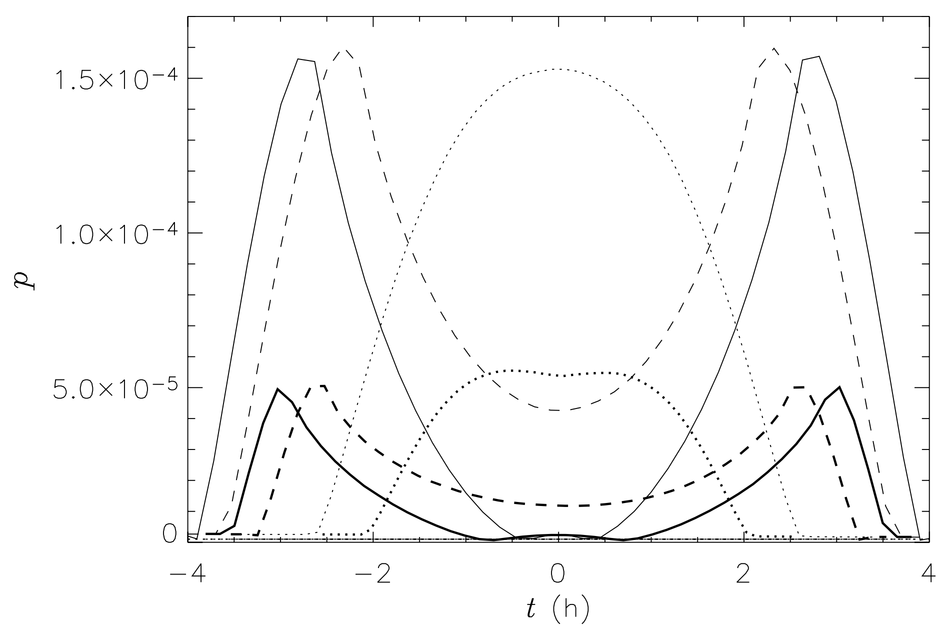

Figure 3.13: Modeled degree of polarization during a transit. Vertical scale is highly model-dependent. This figure is taken from Figure 5 of Carcofi & Magalhães (2005).

to exist at the Ca I $\lambda 4227$ resonant line, and the $P(\lambda) \propto \lambda^{-4}$ dependence of Rayleigh scattering in the stellar photosphere is also present. Thus, our $\approx B$ band instrument is well suited for the detection of a polarized transit. We observed HD 189733 for ≈ 3 hours at Cassegrain ring angle $\phi = 60°$, with ≈ 30 minutes both before and after the transit as well as ≈ 2 hours during the transit. This ring angle was chosen to maximize the polarimetric signal, based on the estimation by B08 of a $\Omega = 16°$ longitude of ascending node. Since the equatorial plane is therefore estimated to have a position angle of $\Theta = 16°$ on the sky, the net polarization of the system (due to the planet outside of transit) is expected to lie at $\Theta = 90° + 16° = 106°$.

During transit ingress and egress, however, position angle of net polarization of the system lies at 45° or 135° with respect to the orbital plane (Figure 3.12). To maximize the sensitivity of POLISH to the transit, we chose to set the Cassegrain ring to $\phi = 45° + 16° \approx 60°$. Note that the use of the Wollaston prism provides equal sensitivity to Stokes components 90° apart. Thus, only the sign of the observed polarization changes whether the transit induces $\Theta = 45°$ or $\Theta = 135°$ polarization with respect to the orbital plane. Subtracting the polarization from each detector enhances the signature of the transit, because the slope of the modulation is opposite for each detector. That is, for system polarization at 45° with respect to the orbital plane, detector 1 will record positive polarization while detector 2 will measure negative polarization. For system polarization at 135° with respect to the orbital plane, the magnitude of the polarization will be the same as for 45°, but the signs will be reversed.

Raw data are shown in Figure 3.14, while Figure 3.15 represents the results after applying a weighted, moving average with a bin size of 79 points. The subscript on the polarization indicates the detector. The dotted boxes in Figure 3.15 represent the uncertainty in polarization as well as the size of the moving average bin. The bin size is chosen to maximize sensitivity to variability at the transit timescale. Since detector 1 observes positive polarization at ingress and negative at egress, while detector 2 observes the opposite, it appears that the planet transits the Southern Hemisphere of the star. This transit appears to have an amplitude of $\Delta P \approx 3 \times 10^{-5}$, which is 1,000 times weaker than the amplitude in photometry.

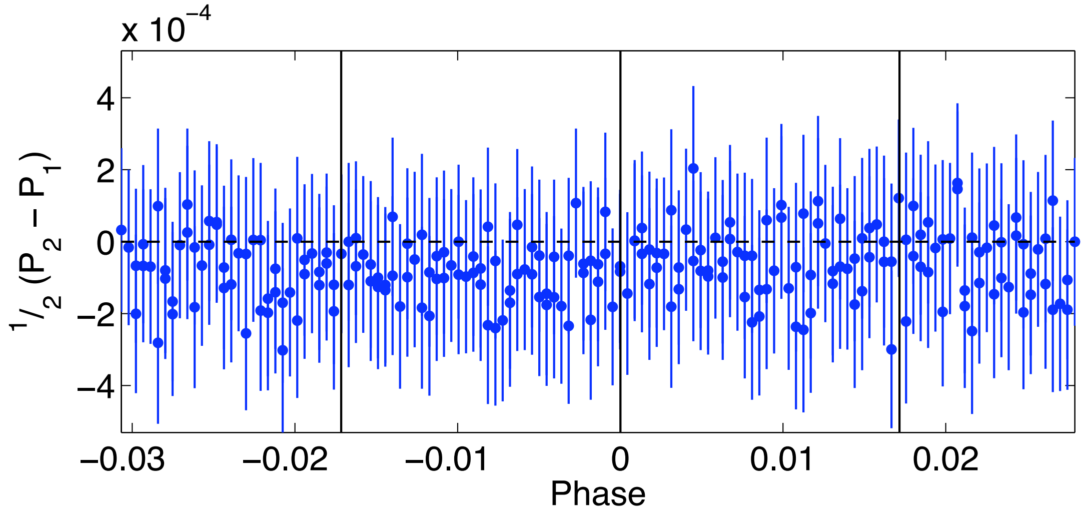

Figure 3.14: Sky-subtracted, polarimetric observations of a transit of the HD 189733 hot Jupiter. The duration of the time series is ≈ 3 hours. Vertical black lines mark transit ingress, mid-transit, and egress.

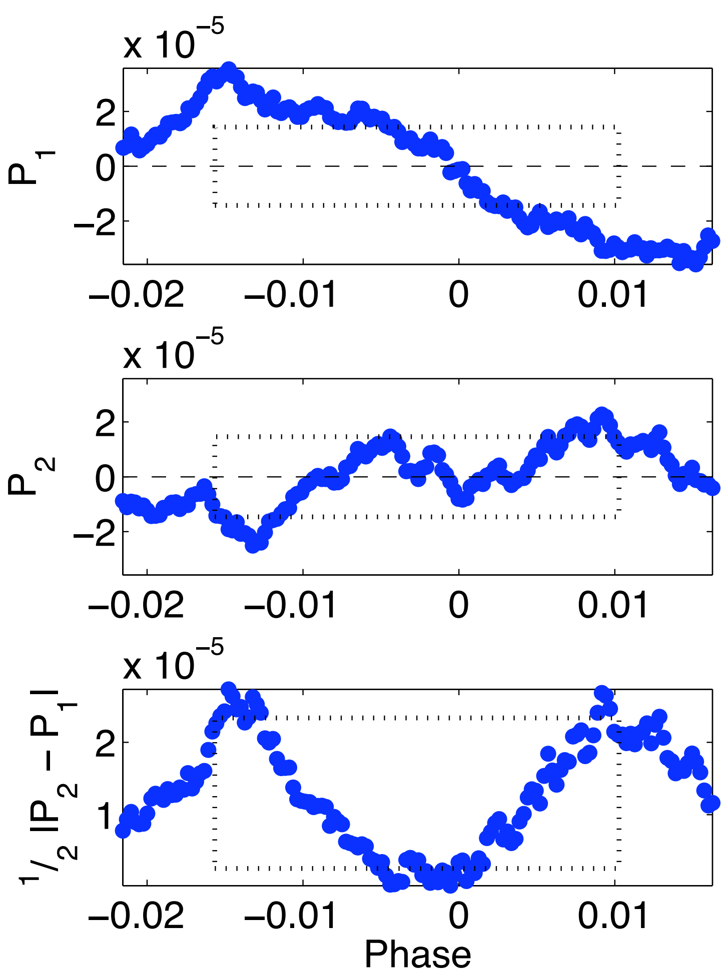

Figure 3.15: Possible transit of an extrasolar planet seen in polarized light. Phase 0 corresponds to mid-transit, and the transit duration is 1.827 hours (Winn et al. 2007).

3.4.3 Debris Disk

γ **Oph (HD 161868, HR 6629).** No variability estimates were found in the literature for this weakly polarized star. It is not significantly variable on one to two night timescales according to Table 3.5. Lack of detected variability is expected due to weak polarization. The minimum ≈ 1 week timescale for ISM variability in the line of sight to γ Oph is approaching the timescale of our observations. Interestingly, marginally significant variability on both a one and two night timescale is observed with detector 1. However, since this is not seen in detector 2, we cannot confirm variability.

γ Oph harbors a debris disk imaged by the Spitzer Space Telescope with inner and outer radii of ≈ 13 and ≈ 520 AU, respectively. This disk, containing 0.010 $M_{\oplus}$ of dust, is inclined at $50 \pm 5°$ with its major axis at a position angle of $55 \pm 2°$ (Su et al. 2008). Multiplying the degree of polarization from Table 3.1 by the 0.836 ± 0.064 correction factor described in section 2, we find absolute polarization of this source to be $P = (1.49 \pm 0.12) \times 10^{-4}$.

To model the expected polarization of the disk, we assume single scattering of the parent star's flux by an optically thin disk composed of small (comparable to the wavelengths of visible light) dust grains. We set γ Oph at the origin O of a right-handed coordinate system. The disk lies on the xy plane, and the observer is along the direction $\theta = i$ (Figure 3.16). Following the derivation in the Appendix (Equations D11a and D11b), the Stokes parameters of the light scattered off the disk are

$$\left(\frac{Q}{I}\right)_{\text{disk}} = \frac{\sin^2 i}{2 + \sin^2 i} \tag{3.8a}$$

$$\left(\frac{U}{I}\right)_{\text{disk}} = 0 \tag{3.8b}$$

which are identical to the expressions of Shakhovskoi (1965). The $+Q$ direction is perpendicular to the disk's major axis for nonzero inclination, and the $-Q$ direction is parallel to the major axis. These Stokes parameters are rotated with respect to celestial north by the position angle of the disk's major axis.

As expected, $(Q/I)_{\text{disk}} = (U/I)_{\text{disk}} = 0$ for $i = 0$. That is, polarization from a face-on disk is zero because of symmetry. For an edge-on disk with $i = \frac{\pi}{2}$, $(Q/I)_{\text{disk}} = \frac{1}{3}$ and $(U/I)_{\text{disk}} = 0$.

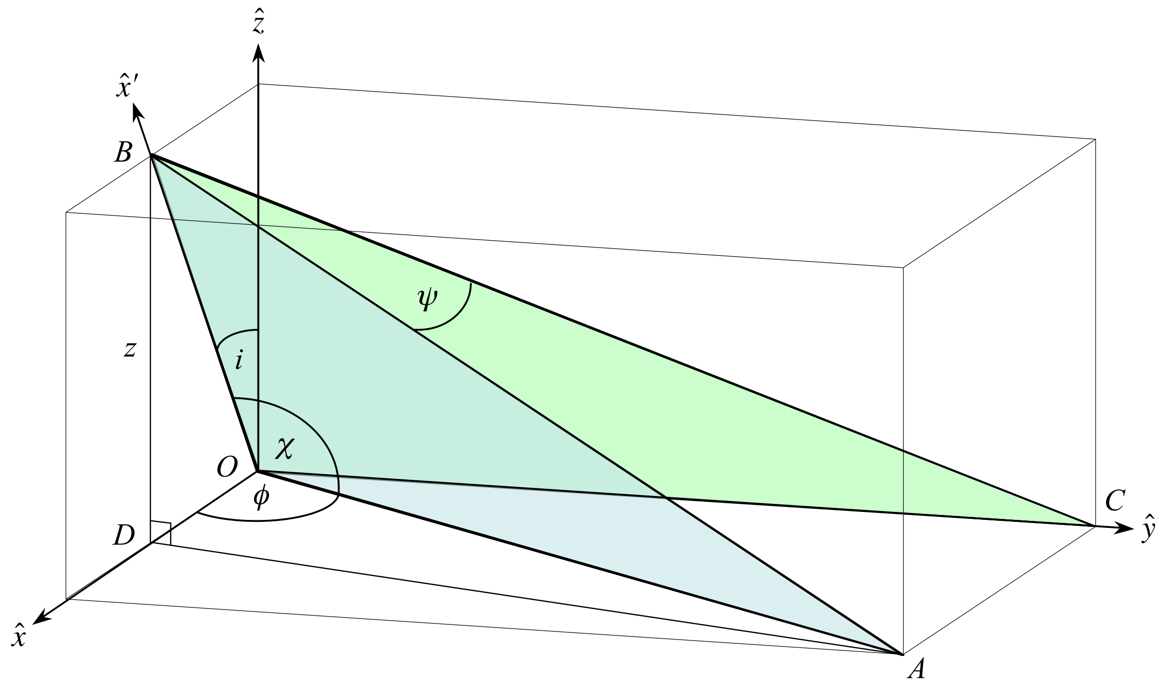

Figure 3.16: Debris disk geometry. The disk is in the xy plane, the blue plane $\overline{OAB}$ is the scattering plane, and the green plane $\overline{OBC}$ is the observer plane.

These results indicate polarization perpendicular to the disk's major axis for all inclination angles, which is predicted by Sunyaev & Titarchuk (1985). Given $i = 50°$ for the γ Oph disk from Su et al. (2008), we find $(Q/I)_{\rm disk} = 0.23$ and $(U/I)_{\rm disk} = 0$ before adding in the star's unpolarized light. Since $(Q/I)_{\rm disk}$ is positive, polarization is expected to be perpendicular to the disk's major axis from single scattering by small particles. However, Table 3.1 shows the position angle of polarization to be $\Theta = 60.56 \pm 0.65°$, while the position angle of the disk's major axis is $\Theta_{\rm disk} = 55 \pm 2°$ (Figure 3.17). Thus, the alignment of the disk polarization with the major axis indicates that either multiple scattering dominates or grain size is large enough for forward-scattering to be dominant.

The latter hypothesis is corroborated by Su et al. (2008), who assume grain sizes ranging from 5 μm to 63 μm based on the spectral energy distribution of the disk. They adopt a constant surface density model for the disk, and the size distribution of the grains is in collisional equilibrium. That is, size distribution is modeled as $n(a) \propto a^{-\frac{7}{2}}$ for grain diameter a. Therefore, the number density of grains as a function of radius in the disk is $n(r) = n_0 \int_{a_{\rm min}}^{a_{\rm max}} a^{-\frac{7}{2}}\, da$, where n_0 is a constant. Assuming grain volume $V(a) = \frac{4}{3}\pi a^3$, their grain density of $\rho = 2.5$ g/cm^3, and disk mass 0.010 $M_\oplus$, we find $n_0 = 2.6 \times 10^{-7}$ from Equation D12. Assuming grain cross-section $\sigma(a) = \pi a^2$, we use Equation D13 to find the fraction of the stellar flux scattered off the disk to be

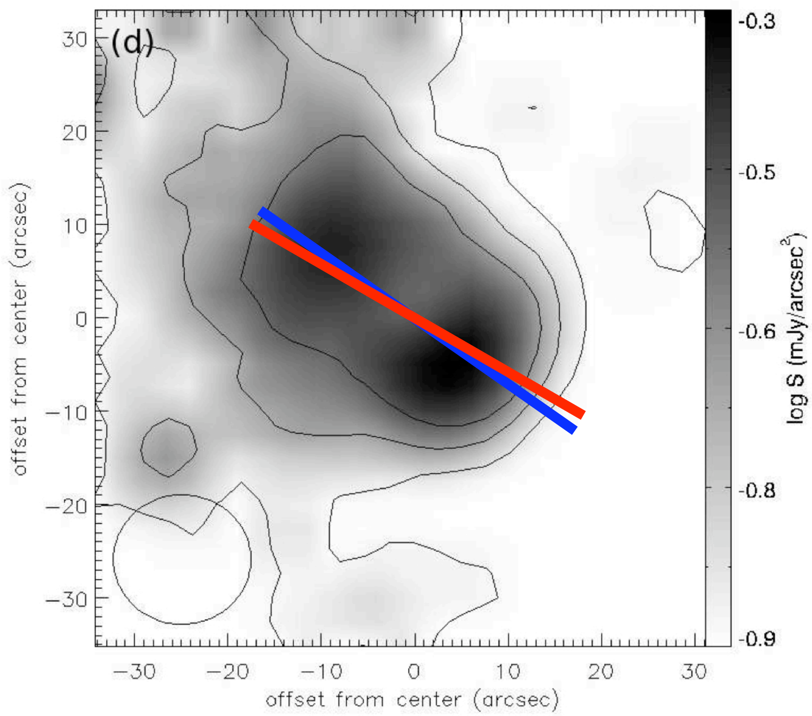

Figure 3.17: Position angle of net polarization, $\Theta = 60.56 \pm 0.65°$ (red line) overlain on a Spitzer image of the γ Oph debris disk (Figure 1d from Su et al. 2008). Position angle of the disk major axis when projected on the sky, $\Theta_{\rm disk} = 55 \pm 2°$, is shown as the blue line.

$$I_{\rm disk} = 2\pi^2 n_0 \left(\frac{1}{\sqrt{a_{\rm min}}} - \frac{1}{\sqrt{a_{\rm max}}} \right) \ln \left(\frac{r_{\rm max}}{r_{\rm min}} \right) \left(2 + \sin^2 i \right) . \qquad (3.9)$$

Here, the inner disk radius is $r_{\rm in}$, and the outer radius is $r_{\rm out}$. Given grain sizes from 5 μm to 63 μm, disk extent 13 to 520 AU, and $i = 50°$ from Su et al. (2008), we find $I_{\rm disk} = 1.6 \times 10^{-3}$. Multiplying this by the expected disk polarization $P_{\rm disk} = \sqrt{(Q/I)^2_{\rm disk} + (U/I)^2_{\rm disk}} = 0.23$ found above, the polarization of the γ Oph system is expected to be $P_{\rm exp} = 4 \times 10^{-4}$. This is the same order of magnitude as the observed polarization $P_{\rm obs} = (1.49 \pm 0.12) \times 10^{-4}$.

Multiple scattering is expected to rotate the polarization position angle by 90° with respect to the single scattering case. This will cause polarization to be parallel to the major axis of the disk (Angel 1969, Sunyaev & Titarchuk 1985, Phillips & Mészáros 1986, Kartje & Königl 1991), as observed. However, multiple scattering tends to decrease the degree of polarization. Since the expected polarization from single scattering is of the same order of magnitude as the observed polarization, multiple scattering cannot be dominant. Thus, the most likely explanation for the alignment of polarimetric position angle and disk major axis is that the grains are predominantly forward-scattering.

Assuming the expected polarization from the single scattering model in Figure 3.16 correctly predicts the system polarization, the slight discrepancies between observed and expected polarization as well as position angle may be due to interstellar polarization. Solving for the interstellar polarization vector necessary to decrease degree of polarization as well as rotate it by 5°, we find $Q_{\rm IP} = (4.6 \pm 2.5) \times 10^{-5}$, $U_{\rm IP} = (-2.11 \pm 0.13) \times 10^{-4}$, $P_{\rm IP} = (2.16 \pm 0.14) \times 10^{-4}$, and $\Theta_{\rm IP} = 141.2 \pm 3.2°$. Uncertainties in interstellar polarization are the minimum possible assuming no uncertainty in expected degree of disk polarization. The probability of random interstellar polarization lying within 86° of the disk's random major axis orientation is 23%, which is not significantly low. Therefore, we posit that the line of sight to γ Oph contains interstellar polarization of degree $P_{\rm IP} \approx 2.2 \times 10^{-4}$ and lying at position angle $\Theta_{\rm IP} \approx 141°$. This degree of interstellar polarization appears to be high when compared with stars at similar distances (Figure 3.6), but γ Oph lies toward the Galactic Center, along with HD 147084 and HD 154445. These stars appear to have enhanced polarization with respect to stars at comparable distances, which is explainable by enhanced dust cloud density along this galactic longitude.

3.4.4 Cepheid Variables

Algenib (γ Peg, HD 886, HR 39). Rudy & Kemp (1978) find circular polarization present and assert a nonzero magnetic field with a null result probability of $\alpha = 0.004$ under the χ^2 test. While no mention is made as to whether this circular polarization could be interstellar in origin, the proximity of this star strongly implies that interstellar polarization, both linear and circular, should be negligible. Thus, the observed circular polarization must be intrinsic to Algenib. No variability estimates were found in the literature for this polarized β Cepheid star.

As with HD 157999, this star appears to be significantly variable in Stokes Q on a one night timescale (Table 3.7), but the signs of variability ΔQ and δQ vary between detectors. Indeed, weighted mean variabilities between detectors, $\Delta Q_{\rm mean}$ and $\delta Q_{\rm mean}$, are not significant. While both APDs have slightly different bandpasses (Figure 3.1), we find no significant difference in position angle between these detectors over the entire run on this star. Thus, it appears that this star may be variable from night to night, but we do not have enough data to state this with much confidence.

The minimum ≈ 1 month timescale for ISM column variability requires that polarimetric variability, if subsequently confirmed, must be intrinsic to the star. The intrinsic circular polarization of the star points to an intrinsic origin for the linear polarization. Indeed, Figure 3.6 implies that the linear polarization in the line of sight to Algenib is an order of magnitude larger than for HD 9270, which is at a similar distance. The polarization maps of Mathewson & Ford (1970) show that HD 9270 and Algenib are both located in the same region of weak polarization in the sky. Therefore, we assert that the linear polarization seen in Algenib is intrinsic to the star.

The position angle of net polarization for Algenib is $\Theta = 111°$ from Table 3.1, so its $P \approx 1\%$ polarization is split fairly evenly between Stokes Q and U. This is because Stokes $+Q$ is projected north/south on the sky ($\Theta = 0°/180°$), Stokes $-Q$ is east/west ($\Theta = 90°/270°$), Stokes $+U$ is northeast/southwest ($\Theta = 45°/225°$), and Stokes $-U$ is northwest/southeast ($\Theta = 315°/135°$). One might therefore expect that variability in Algenib would occur with equal amplitude in both Stokes Q and U. Reasons for stronger variability in Stokes Q as opposed to U are unknown.

HD 187929 (η Aql, HR 7570). Serkowski et al. (1975) find polarization as a function of wavelength of this δ Cepheid variable to be consistent with interstellar origin. Dolan & Tapia (1986) and Clarke (1986) independently discovered changes in polarimetric position angle with wavelength, and this result has been confirmed by Wolff et al. (1996). The probability of constant position angle versus wavelength is $\alpha < 10^{-5}$ according to the χ^2 test (Dolan & Tapia 1986). However, Stokes et al. (1974) and Wade et al. (2002) do not detect significant circular polarization of this star. Therefore, some linear polarization must be intrinsic to the star, because rotation of position angle with respect to wavelength cannot be due to dust grain rotation along the line of sight. Polarimetric variability is inconclusive according to Dolan & Tapia (1986), "suspected" by Bastien et al. (1988), and rejected by both Clarke & Naghizadeh-Khouei (1994) and the Bastien et al. (2007) reanalysis of Bastien et al. (1988) data.

However, we detect strong variability in both Stokes parameters on a two night timescale, as $\Delta Q, U_{\mathrm{mean}}$ and $\delta Q, U_{\mathrm{mean}}$ are much larger than three times their respective uncertainties. The sign of variability on a one night timescale varies between detector, so it is difficult to claim variability on this timescale with confidence. While the variability in Stokes Q on a three night timescale has different sign between detector 1 and detector 2, variability in Stokes U on this timescale has the same sign. As with variability of this star on a one night timescale, variability on a three night timescale is difficult to claim without more data.

It is possible that changes in variability occur with wavelength, since changes in position angle are known to occur with wavelength. While both APDs have slightly different bandpasses (Figure 3.1), we find no significant difference in position angle between these detectors over the entire run on this star. According to Table 3.10, the minimum timescale for ISM variability along the line of sight to this star is ≈ 4 months. In addition, the observed variability in Stokes Q is only ≈ 3 times larger than that in Stokes U, even though run-averaged Stokes Q is ≈ 10 times larger than Stokes U. One would expect that a random orientation of the system in the plane of the sky would cause intrinsic polarization variability to occur with roughly equal amplitude in each Stokes parameter. However, variability in interstellar polarization would be expected to be stronger in the dominant Stokes parameter. Thus, the variability of this star must be caused by changes in its intrinsic polarization.

The period of this Cepheid variable is $T \approx 7.2$ days (Gray & Stevenson 2007). Even though Cepheids are radial pulsators, there must be some asymmetry in the distribution of scatterers in the star's envelope to introduce time-variable, intrinsic polarization. Indeed, polarimetric monitoring of post-AGB stars has shown pulsation phase-locked variability that is generally explained by non-radial pulsations (Henson et al. 1985, Magalhães et al. 1986, Raveendran & Rao 1989, Yudin & Evans 2002). Trammell et al. (1994), on the other hand, suggest polarimetric varaibility to be caused by clumpy mass loss. From ephemerides in Table 2 of Gray & Stevenson (2007), our observations on UT 2007 Aug 3, 5, and 6 were taken at phases 0.013 to 0.018, 0.296 to 0.298, and 0.436 to 0.438, respectively. Maximum negative radial velocity is achieved at phase ≈ 0.05, zero radial velocity at phase 0.5, and maximum positive radial velocity occurs at phase ≈ 0.8. Thus, our observations almost completely bracket the ranges of increasing radial velocity from maximum negative radial velocity to its first zero crossing.

Variations in polarization are plotted against pulsation phase in Figure 3.18. While the data for UT 2007 Aug 6 (phase 0.44) are inconsistent from detector to detector, the positive increase in polarization between UT 2007 Aug 3 and 5 (phases 0.02 and 0.30) is clear. Net polarization, $P = \sqrt{Q/I^2 + U/I^2}$, decreases between these two nights when the star's change in size is at a maximum.

From Sudzius (1969) and Depenchuk (1980), the star dims by $\Delta V \approx 0.34$ mag, or 27%, between these phases. From Table 3.14, we see a strong, *relative* decrease in polarization of $\delta P =$

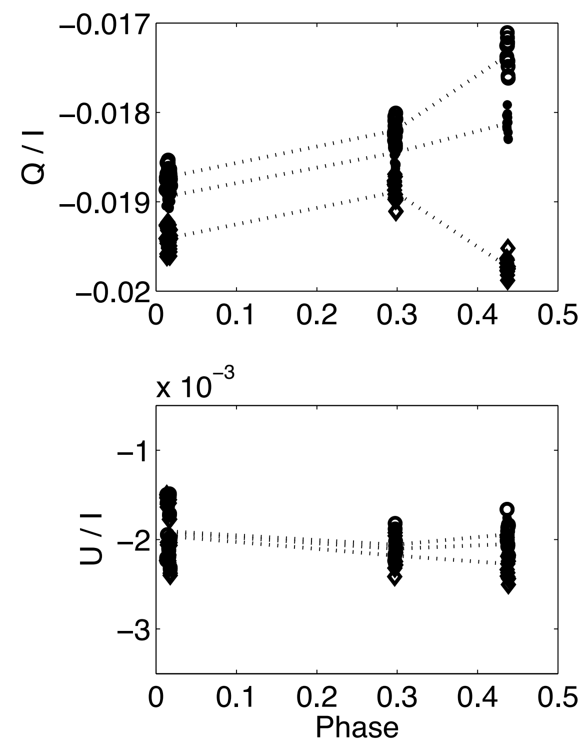

Figure 3.18: Polarization variations in HD 187929 versus Cepheid pulsation phase. Open circles are data from detector 1, open diamonds are from detector 2, and filled circles are weighted mean measurements from both detectors ("detector 1,2"). Dotted lines are guides for the eye.

Table 3.14: HD 187929 Variability

Detector	ΔP ($\times 10^{-6}$)	δP (%)	$\Delta\Theta$ (°)
1	−490(35)	−2.60(18)	0.32(13)
2	−485(39)	−2.49(20)	0.35(13)
Mean	−487.8(2.5)	−2.550(59)	0.336(12)

$2.550 \pm 0.059\%$ and a weak, *absolute* increase in position angle $\Delta\Theta = 0.336 \pm 0.012°$ in this time interval. Thus, it appears that the radial increase in size of the star dampens the intrinsic polarization, because a change in stellar intensity should have no effect on polarization. This is because the Stokes parameters Q and U are normalized by the Stokes I intensity parameter.

3.5 Conclusion

We have observed no conclusive polarimetric variability with timescales less than four nights on stars with polarization $P < 2\%$. No star, even the famously variable Cygnus X-1, exhibits detectable polarimetric variability during a single night. We have observed no significant variability of the long period extrasolar planet host star HR 8974, which has a period $T \approx 2.5$ years. However, there is weak, qualitative evidence for long period variability in HD 175541, which harbors a long period extrasolar planet with $T \approx 10$ months. The polarization expected from the planets in these systems is less than one part in 10^7, so observed variability must be due to stochastic variability in the host star itself. No phase-locked behavior is observed for the transiting extrasolar planet system HD 149026, and we do not detect significant variability of the HD 189733 transiting system. Marginal variability in this system is claimed by Berdyugina et al. (2008).

We present tentative evidence for a transit of HD 189733 in polarized light, which is the first reported observation of this effect. The characteristic double-peaked profile predicted by Carciofi & Magalhães (2005), due to occultation of stellar limb polarized, is observed. The transit depth appears to be $\Delta P \approx 3 \times 10^{-5}$, which is three orders of magnitude weaker than seen in photometry (Winn et al. 2007). Polarimetry provides additional geometric information that is difficult to determine from photometric transits. For instance, our observations imply a Southern Hemisphere transit by the planet due to the observed sign of rotation of the polarization vector.

The polarized light scattered by the γ Oph debris disk has been detected, and its position angle is closely aligned to the disk's major axis when projected on the sky. This is evidence for an optically thin disk composed of predominantly forward-scattering dust grains, which must therefore be larger than the wavelengths of visible light. In addition, we find evidence that the line of sight to this nearby star contains interstellar polarization of an order of magnitude larger than do stars at similar distances and along other sightlines. This is consistent with galactic longitude of this star near the Galactic Center.

Polarimetric variability of the β Cepheid pulsator Algenib is observed at low significance. There exists significant circular polarization intrinsic to this star (Rudy & Kemp 1978), which suggests that linear polarimetric variability should also be present. A longer temporal baseline of polarimetric observations is therefore desired. We have confirmed the suspected polarimetric variability of the δ Cepheid star HD 187929 on a two night timescale, which represents $\approx 30\%$ of the pulsation phase. Indeed, this star is known to harbor significant intrinsic linear polarization (Dolan & Tapia 1986, Clarke 1986). While Cepheid variables are radial pulsators, temporal variability of intrinsic linear polarization indicates time-variable asymmetry in the system. Degree of polarization of this star decreases as stellar radius increases, which is likely due to an increase in symmetry of the system. We confirm polarimetric variability of HD 204827, for which the community position is inconclusive. Nightly variability in the control system, Cygnus X-1, is confirmed to high significance. The next chapter will describe in detail observations of Cygnus X-1.

References

Angel, J. R. P. 1969, ApJ 158, 219.

Aspin, C., Simmons, J. F. L., & Brown, J. C. 1981, MNRAS 194, 283.

Bailey, J. & Hough, J. H. 1982, PASP 94, 618.

Baines, E. K., van Belle, G. T., ten Brummelaar, T. A., McAlister, H. A., Swain, M., Turner, N. H., Sturmann, L., & Sturmann, J. 2007, ApJ 661, L195.

Bastien, P., Drissen, L., Menard, F., Moffat, A. F. J., Robert, C. & St-Louis, N. 1988, AJ 95, 900.

Bastien, P., Vernet, E., Drissen, L., Ménard, F., Moffat, A. F. J., Robert, C., & St-Louis, N. 2007, ASP Conf. Ser. 364, 529.

Batten, A. H. 1967, Pub. Dom. Ap. Obs. 13, 162.

Berdyugina, S. V., Berdugin, A. V., Fluri, D. M., & Piirola, V. 2008, ApJ 673, L83.

Carciofi, A. C. & Magalhães, A. M. 2005, ApJ 635, 570.

Clarke, D. 1986, A&A 156, 213.

Clarke, D. & Naghizadeh-Khouei, J. 1994, AJ 108, 687.

Clayton, G. C., Wolff, M. J., Allen, R. G. & Lupie, O. L. 1995, ApJ 445, 947.

Coyne, G. V. & Gehrels, T. 1966, AJ 71, 355.

Croll, B., Matthews, J. M., Rowe, J. F., Gladman, B., Miller-Ricci, E., Sasselov, D., Walker, G. A. H., Kuschnig, R., Lin, D. N. C., Guenther, D. B., Moffat, A. F. J., Rucinski, S. M., & Weiss, W. W. 2007, ApJ 671, 2129.

Croll, B., Matthews, J. M., Walker, G. A. H., Rowe, J. F., Miller-Ricci, E., Kuschnig, R., Sasselov, D., Rucinski, S., Walker, A., Guenther, D. B., Moffat, A. F. J., & Weiss, W. W. 2008, ApJ, submitted.

Davis, L., Jr. & Greenstein, J. L. 1951, ApJ 114, 206.

Depenchuk, E. A. 1980, IAU 1819, 1.

Dolan, J. F. & Tapia, S. 1986, PASP 98, 792.

Dolan, J. F. & Tapia, S. 1989, ApJ 344, 830.

Gehrels, T. 1972. ApJ 173, L23.

Gehrels, T. & Silvester, A. B. 1965. AJ 70, 579.

Gies, D. R., Bolton, C. T., Thomson, J. R., Huang, W., McSwain, M. V., Riddle, R. L., Wang, Z., Wiita, P. J., Wingert, D. W., Csák, B., & Kiss, L. L. 2003, ApJ 583, 424.

Gray, D. F. & Stevenson, K. B. 2007, PASP 119, 398.

Hatzes, A. P., Cochran, W. D., Endl, M., McArthur, B., Paulson, D. B., Walker, G. A. H., Campbell, B., & Yang, S. 2003, ApJ 599, 1383.

Hébrard, G. & Lecavelier des Etangs, A. 2006, A&A 445, 341.

Heiles, C. 2000, AJ 119, 923.

Henry, G. W. & Winn, J. N. 2008, AJ 135, 68.

Henson, G. D., Kemp, J. C., & Kraus, D. J. 1985, PASP 97, 1192.

Hsu, J.-C. & Breger, M. 1982, ApJ 262, 732.

Johnson, J. A., Fischer, D. A., Marcy, G. W., Wright, J. T., Driscoll, P., Butler, R. P., Hekker, S., Reffert, S., & Vogt, S. S. 2007, ApJ 665, 785.

Kartje, J. F. & Königl, A. 1991, ApJ 375, 69.

Kemp, J. C. 1972, ApJ 175, L35.

Kemp, J. C. & Wolstencroft, R. D. 1972, ApJ 176, L115.

Kemp, J. C., Barbour, M. S., Parker, T. E., & Herman, L. C. 1979, ApJ 228, 23.

Kemp, J. C., Henson, G. D., Steiner, C. T., Powell, E. R. 1987, Nature 326, 270.

Kovachev, B. J. & Reinhardt, M. 1975, Acta Astr. 25, 133.

Kukarkin, B. V. Parenago, P. P., Efremov, Y. I., & Kholopov, P. N. 1958, in *General catalogue of Variable Stars*. Academy of Science USSR, Moscow.

Leigh, C., Cameron, Andrew C., Horne, K., Penny, A., & James, D. 2003, MNRAS 344, 1271.

Magalhães, A. M., Coyne, G. V., Codina-Landaberry, S. J., & Gneiding, C. 1986, A&A 154, 1.

Martin, P. G. 1974, ApJ 187, 461.

Massey, P., Johnson, K. E., & DeGioia-Eastwood, K. 1995, ApJ 454, 151.

Mathewson, D. S., & Ford, V. L. 1970, Mem. RAS 74, 139.

Merril, J. E. 1963, in *Photoelectric Astronomy for Amateurs*, ed. F. B. Wood. Macmillan, New York, p. 176.

Moutou, C., Donati, J.-F., Savalle, R., Hussain, G., Alecian, E., Bouchy, F., Catala, C., Collier Cameron, A., Udry, S., & Vidal-Madjar, A. 2008, A&A 473, 651.

Neuhäuser, R., Mugrauer, M., Fukugawa, M., Torres, G., & Schmidt, T. 2007, A&A 462, 777.

Nutzman, P., Charbonneau, D., Winn, J. N., Knutson, H. A., Fortney, J. J., Holman, M. J., Agol, E. 2008, arXiv:0805.0777.

Ochsenbein, F., Bauer, P., & Marcout, J. 2000, A& AS 143, 221.

Oke, J. B. 1961, ApJ 133, 90.

Pasinetti-Fracassini, L. E., Pastori, L., Covino, S., & Pozzi A. 2001, A&A 367, 521.

Phillips, K. C. & Mészáros, P. 1986, ApJ 310, 284.

Pont, F., Gilliland, R. L., Moutou, C., Charbonneau, D., Bouchy, F., Brown, T. M., Mayor, M., Queloz, D., Santos, N., & Udry, S. 2007, A&A 476, 1347.

Raveendran, A. V. & Rao, N. K. 1989, A&A 215, 63.

Rudy, R. J. & Kemp, J. C. 1977, ApJ 216, 767.

Rudy, R. J. & Kemp, J. C. 1978, MNRAS 183, 595.

Schmidt, G. D., Elston, R., Lupie, O. L. 1992, AJ 104, 1563.

Schulz, A. & Lenzen, R. 1983, A&A 121, 158.

Seager, S., Whitney, B. A., & Sasselov, D. D. 2000, ApJ 540, 504.

Serkowski, K. 1962, Adv. Astr. & Ap. 1, 289.

Serkowski, K. 1968, ApJ 154, 115.

Serkowski, K., Mathewson, D. S., & Ford, V. L. 1975, ApJ 196, 261.

Shakhovskoi, N. M. 1965, SvA 8, 833.

Shkolnik, E., Walker, G. A. H., Bohlender, D. A., Gu, P.-G., & Kúrster, M. 2005, ApJ 622, 1075.

Shkolnik, E., Bohlender, D. A., Walker, G. A. H., & Collier Cameron, A. 2008, ApJ 676, 628.

Stokes, R. A., Swedlund, J. B., Avery, R. W., & Michalsky, J. J. 1974, AJ 79, 6.

Sudzius, J. 1969, Viln. Astron. Obs. Biul. 26, 23.

Su, K. Y. L., Rieke, G. H., Stapelfeldt, K. R., Smith, P. S., Bryden, G., Chen, C. H., & Trilling, D. E. 2008, ApJ 679, L125.

Sunyaev, R. A. & Titarchuk, L. G. 1985, A&A 143, 374.

Trammell, S. R., Dinerstein, H. L., & Goodrich, R. W. 1994, AJ 108, 984.

Wade, G. A., Chadid, M., Shorlin, S. L. S., Bagnulo, S., & Weiss, W. W. 2002, A&A 392, L17.

Walker, G. A. H., Croll, B., Matthews, J. M., Kuschnig, R., Huber, D., Weiss, W. W., Shkolnik, E., Rucinski, S. M., Guenther, D. B., Moffat, A. F. J., & Sasselov, D. 2008, A&A 482, 691.

Winn, J. N., Holman, M. J., Henry, G. W., Roussanova, A., Enya, K., Yoshii, Y., Shporer, A., Mazeh, T., Johnson, J. A., Narita, N., & Suto, Y. 2007, AJ 133, 1828.

Winn, J. N., Henry, G. W., Torres, G., & Holman, M. J. 2008, ApJ 675, 1531.

Wolff, M. J., Nordsieck, K. H., & Nook, M. A. 1996, AJ 111, 856.

Wolinski, K. G., Dolan, J. F., Boyd, P. T., Biggs, J. D., Nelson, M. J., Percival, J. W., Taylor, M., & van Citters, G. W. 1996, ApJ 457, 859.

Yudin, R. V. & Evans, A. 2002, A&A 391, 625.

Ziólkowski, J. 2005, MNRAS 358, 851.

3.6 Appendix D: Single Scattering Geometry

Consider a right handed coordinate system (x, y, z) with the observer along the x' axis, which is inclined at an angle i with respect to the x axis (Figure 3.16). An infinitesimally thin debris disk lies along the xy plane, and the central star illuminates the disk from the origin. For a dust grain located at point A, photons will be scattered through an angle χ (the angle between the radius vector and the x' axis). The scattering plane contains the star, dust grain, and the observer. The electric field of scattered light will be perpendicular to this plane for particles smaller than the wavelengths of incident light. The $x'y$ plane and the scattering plane intersect along the x' axis, and the angle between them is ψ. The Stokes parameters of photons scattered off the grain are given by

$$\begin{pmatrix} I_{\text{grain}} \\ Q_{\text{grain}} \\ U_{\text{grain}} \end{pmatrix} = \sigma \begin{pmatrix} 1 + \cos^2 \chi \\ \sin^2 \chi \cos 2\psi \\ \sin^2 \chi \sin 2\psi \end{pmatrix} \tag{D1}$$

where σ is the scattering cross section of the grain.

To find angle χ in terms of ϕ and i, we note

$$\overline{AB}^2 = z^2 + \overline{AD}^2 = z^2 + A_x'^2 + r^2 - 2rA_x' \cos \phi \tag{D2a}$$

$$\overline{AB}^2 = r^2 + \overline{OB}^2 - 2r\overline{OB} \cos \chi. \tag{D2b}$$

Equating Equations D2a and D2b and noting $z^2 + A_x'^2 = \overline{OB}^2$,

$$A_x' \cos \phi = \overline{OB} \cos \chi. \tag{D3}$$

Since

$$\tan i = \frac{A_x'}{z} \tag{D4a}$$

$$\sec i = \frac{\overline{OB}}{z} \tag{D4b}$$

we arrive at

$$\cos \chi = \cos \phi \sin i. \tag{D5}$$

To find angle ψ we first find the vectors normal to both the scattering and $x'y$ planes. The scattering plane contains vectors $\overrightarrow{OB} = (A'_x, 0, z)$ and $\overrightarrow{OA} = (A_x, A_y, 0)$, while the $x'y$ plane contains vectors $\overrightarrow{OB}$ and $\overrightarrow{OC} = (0, A_y, 0)$. Therefore, vectors normal to the scattering plane, $\overrightarrow{n_s}$, and to the $x'y$ axis, $\overrightarrow{n_x}$, are

$$\overrightarrow{n_s} = \overrightarrow{OB} \times \overrightarrow{OA} = (-A_y z, A_x z, A'_x A_y) \tag{D6a}$$

$$\overrightarrow{n_x} = \overrightarrow{OB} \times \overrightarrow{OC} = (-A_y z, 0, A'_x A_y)\,. \tag{D6b}$$

Finally, the angle between these vectors is given by

$$\cos\psi = \frac{\overrightarrow{n_s} \cdot \overrightarrow{n_x}}{|\overrightarrow{n_s}|\,|\overrightarrow{n_s}|} = \left\{ \frac{z^2 + A_x'^2}{z^2 \left[1 + \left(\frac{A_x}{A_y}\right)^2\right] + A_x'^2} \right\}^{\frac{1}{2}} \tag{D7a}$$

$$\cos\psi = \left(\cot^2\phi \cos^2 i + 1\right)^{-\frac{1}{2}}\,. \tag{D7b}$$

For an ensemble of grains located at $\theta = \frac{\pi}{2}$, Equation D1 becomes

$$\begin{pmatrix} I_{\text{disk}} \\ Q_{\text{disk}} \\ U_{\text{disk}} \end{pmatrix} = \sigma \int_0^{2\pi} \int_{r_{\text{in}}}^{r_{\text{out}}} \frac{n(r)}{r^2} \begin{pmatrix} 1 + \cos^2\chi \\ \sin^2\chi \cos 2\psi \\ \sin^2\chi \sin 2\psi \end{pmatrix} r dr d\phi. \tag{D8}$$

We are interested in the normalized Stokes parameters $(Q/I)_{\text{disk}}$ and $(U/I)_{\text{disk}}$. Since neither χ nor ψ depends on the radius r, we have

$$I_{\text{disk}} = R_0 \int_0^{2\pi} 1 + \cos^2\chi \; d\phi \tag{D9a}$$

$$Q_{\text{disk}} = R_0 \int_0^{2\pi} \sin^2\chi \cos 2\psi \; d\phi \tag{D9b}$$

$$U_{\text{disk}} = R_0 \int_0^{2\pi} \sin^2\chi \sin 2\psi \; d\phi \tag{D9c}$$

$$R_0 = \sigma \int_{r_{\text{in}}}^{r_{\text{out}}} \frac{n\,(r)}{r} \; dr. \tag{D9d}$$

Given χ and ψ from Equations D5 and D7b,

$$I_{\rm disk} = R_0 \int_0^{2\pi} 1 + \cos^2\phi \sin^2 i \; d\phi = \pi R_0 \left(2 + \sin^2 i\right) \tag{D10a}$$

$$Q_{\rm disk} = R_0 \int_0^{2\pi} \sin^2\phi - \cos^2\phi \cos^2 i \; d\phi = \pi R_0 \sin^2 i \tag{D10b}$$

$$U_{\rm disk} = R_0 \int_0^{2\pi} \sin 2\phi \cos i \; d\phi = 0. \tag{D10c}$$

Thus, we derive the relations of Shakhovskoi (1965) describing the single-scattering polarization of a disk illuminated centrally:

$$\left(\frac{Q}{I}\right)_{\rm disk} = \frac{\sin^2 i}{2 + \sin^2 i} \tag{D11a}$$

$$\left(\frac{U}{I}\right)_{\rm disk} = 0. \tag{D11b}$$

Because the inclination terms in Equation D11a are squared, polarimetry is unable to distinguish between inclinations $\pm i$.

To estimate the single-scattering polarization when unpolarized light from the central star is added to the polarized light from the disk, we need the number density of dust grains $n(r,a)$. The disk mass is

$$M = \int_{r_{\rm in}}^{r_{\rm out}} \int_{a_{\rm min}}^{a_{\rm max}} 2\pi r \; n(r,a) \; V(a) \; \rho \; dadr \tag{D12}$$

for grain volume and density $V(a)$ and ρ. We assume $n(r,a) = n_0 n(r) n(a)$, where a is grain diameter and n_0 is a constant. From Equations D10a and D9d, the fraction of the stellar flux reflected by the disk is

$$I = n_0 \int_0^{2\pi} \int_{r_{\rm in}}^{r_{\rm out}} \int_{a_{\rm min}}^{a_{\rm max}} \frac{\sigma(a) \; n(r) \; n(a)}{r} \left(1 + \cos^2\phi \sin^2 i\right) dadrd\phi. \tag{D13}$$